

## A MODEL FOR THE PHYSICAL ADSORPTION OF ATOMIC HYDROGEN

L.W. BRUCH \* and Th.W. RUIJGROK

*Instituut voor Theoretische Fysica, Rijksuniversiteit Utrecht, Utrecht, The Netherlands*

Received 30 May 1978; manuscript received in final form 16 August 1978

The formation of the holding potential of physical adsorption is studied with a model in which a hydrogen atom interacts with a perfectly imaging substrate bounded by a sharp planar surface; the exclusion of the atomic electron from the substrate is an important boundary condition in the model. The interaction energy and the dipole and quadrupole moments of the ground state are determined with a variational calculation. The polarizability tensor of the ground state and the interaction energies in the first few excited states are also determined. A quantitative analysis is given of the transition to the dispersion-force, large-separation regime using results of perturbation theory and of the variational solution for the ground state of a hydrogen atom in the presence of a nonimaging wall. The relation of results for the image model to ideas used in the modelling of experiments is discussed; this includes a treatment of image field contributions to the depolarizing field at an adatom.

### 1. Introduction

In this paper we report the results of calculations of an idealized model for the physical adsorption of a hydrogen atom: a hydrogen atom in the presence of a perfectly imaging semi-infinite metal [1,2]. The simplifications made in the construction of the model enable us to give an accurate account of its content. It provides a concrete illustration of the balancing of the contributions of different intermolecular force mechanisms in the adsorption energy and in properties of the ground state of the adatom–substrate complex. The analysis of this model may be a useful preliminary to detailed treatments of adsorption which would include correlation effects between the electrons of the adatom and the metal [3–6].

The holding potential of an adatom to a surface in physical adsorption is thought [3–10] to be formed by a balance between an attractive dispersion force and an exchange repulsion arising from the overlap of adatom and substrate electrons. To improve upon this qualitative understanding, it is desirable to have a

\* Permanent address: Department of Physics, University of Wisconsin–Madison, Madison, Wisconsin 53706, USA. Work of this author is supported in part by the Wisconsin Alumni Research Foundation.

model where the balance between these two processes can be traced as a function of separation, and for which a local minimum is formed in the holding potential. For our model we trace the balance in the interaction energy and in such derived properties as the dipole and quadrupole moments of the adatom and in its polarizability.

We reduce the many-electron problem of adsorption theory [3–6] to a one-electron problem by introducing several simplifying assumptions. The electrodynamic response of the substrate is specified by a continuum dielectric constant, which is a considerable simplification even for a perturbation theory treatment [11]. Our model does not include the intermingling of adatom and substrate electrons which occurs in chemisorption [3,4].

The interaction of a hydrogen atom with a metal modelled by jellium has been studied in other works recently [6–8]. Compared to such work, our model has the defect of being less realistic physically, but it has the advantage that our treatment can be more transparent and more complete.

The paper is organized in ten sections and an Appendix which are grouped as follows: Section 2 contains the statement of the model, definitions of the coordinate system, and a discussion of the assumptions made in constructing the model. Sections 3 through 5 contain treatments of the model in the limits of large and small adatom–surface separations; these establish the framework in which the later results are discussed. In section 3, qualitative features of the interaction energy are established. Perturbation theory results for large separations are reviewed and extended in section 4. A variational calculation for small separations is presented in section 5. The principal body of detailed results is contained in sections 6 through 8. The results of a large scale variational calculation of the ground state and the first few excited states are presented in section 6. In section 7 these results are compared with the results of section 4 to give a quantitative analysis of the transition to the large-separation dispersion-theory regime. Section 8 contains the treatment of the polarizability tensor of the system. Several of the results may be useful in the discussion and analysis of experiments on physisorbed atoms. We collect some of this information in section 9, including the energy level spectrum for atomic motion in the holding potential and the results of a calculation for a finite dielectric constant. We present our conclusions and a summary in section 10. We include an Appendix which shows the role of image-charge fields in determining the dipole moment of an adatom; this is a rederivation of a result of Antoniewicz [12].

## 2. The model

We determine properties of a hydrogen atom interacting with a perfectly imaging semi-infinite metal with a sharp planar surface [1,2].

The proton is at a perpendicular distance  $L$  from the (non-diffuse) surface and the instantaneous potential energy is the sum of the Coulomb interactions. The geometry is shown in fig. 1.

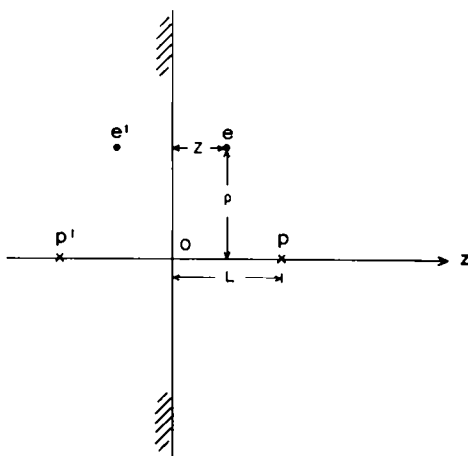


Fig. 1. Coordinate system for the adsorbed hydrogen atom. The figure shows the relative positions of charges and images for the proton ( $p$  and  $p'$ ) and the electron ( $e$  and  $e'$ ). The basic cylindrical coordinate system is also indicated.

## 2.1. Coordinate systems

Three coordinate systems are used to describe the positions of the charges. Each leads to considerable simplifications in parts of our treatment.

The basic system is indicated in fig. 1: cylindrical coordinates with the polar  $z$  axis going from position of the image-proton to the proton and with the origin of coordinates at the intersection of the polar axis with the planar substrate surface. The lateral distance from the polar axis is denoted  $\rho$  and the azimuthal angle is denoted  $\phi$ .

A second coordinate system is used in defining multipole moments of the adatom charge distribution and in the perturbation theory of section 4. The cylindrical coordinates just described are used with the origin of coordinates taken at the proton. Then the coordinate  $z$  is replaced by a  $\zeta$  variable which is related to it by

$$\zeta = z - L, \quad (2.1)$$

and the distance from the electron to the proton is

$$r = \{\rho^2 + \zeta^2\}^{1/2}. \quad (2.2)$$

The third coordinate system is used in the variational solution of the Schrödinger equation in section 6: confocal elliptic coordinates [13] with foci at the proton and image proton. The coordinates  $\xi$  and  $\eta$  are defined in terms of the

first set of coordinates by

$$\xi = [\{\rho^2 + (z - L)^2\}^{1/2} + \{\rho^2 + (z + L)^2\}^{1/2}] / 2L, \quad (2.3)$$

$$\eta = [\{\rho^2 + (z + L)^2\}^{1/2} - \{\rho^2 + (z - L)^2\}^{1/2}] / 2L. \quad (2.4)$$

The azimuthal angle  $\phi$  remains as before. Then the element of volume is

$$\rho \, d\rho \, dz \, d\phi = L^3 (\xi^2 - \eta^2) \, d\xi \, d\eta \, d\phi, \quad (2.5)$$

and the Laplacian is [13]

$$\nabla^2 = [L^2(\xi^2 - \eta^2)]^{-1} \left\{ \frac{\partial}{\partial \xi} (\xi^2 - 1) \frac{\partial}{\partial \xi} + \frac{\partial}{\partial \eta} (1 - \eta^2) \frac{\partial}{\partial \eta} + \frac{(\xi^2 - \eta^2)}{(\xi^2 - 1)(1 - \eta^2)} \frac{\partial^2}{\partial \phi^2} \right\}. \quad (2.6)$$

In the half-space  $z \geq 0$ , the ranges of the coordinates  $\xi$  and  $\eta$  are

$$1 \leq \xi \leq \infty, \quad 0 \leq \eta \leq 1. \quad (2.7)$$

## 2.2. Hamiltonian and observables

The Hamiltonian is composed of the kinetic energy of the atomic electron and the Coulomb electrostatic energy of the proton, the atomic electron and their images (fig. 1).

The atomic electron is assumed to be excluded from the interior of the metal so that its accessible space is the half-space  $z \geq 0$ .

The adatom-metal interaction energy (holding potential) and the ground-state electron distribution are obtained in the Born-Oppenheimer approximation [13] by solving the Schrödinger equation for the ground state of the atomic electron as a function of the proton-metal distance  $L$ :

$$H\psi_0 = E_0\psi_0, \quad (2.8)$$

$$H = K + V, \quad (2.9)$$

$$K = -\frac{1}{2}\nabla^2, \quad (2.10)$$

$$V = -\{\rho^2 + (z - L)^2\}^{-1/2} + \{\rho^2 + (z + L)^2\}^{-1/2} - 1/(4L) - 1/(4z) \\ \equiv -1/r + V_i(\rho, z; L), \quad (2.11)$$

$$\psi_0 = 0, \quad z \leq 0. \quad (2.12)$$

Atomic units are used throughout this paper: the electron mass  $m$ , the magnitude of electron charge and the reduced Planck constant are all set equal to unity. The unit of distance is 1 bohr,  $1 a_0 \approx 0.529 \text{ \AA}$ , and the unit of energy is 1 hartree,  $e^2/a_0 \approx 27.2 \text{ eV}$ . In these units the ground state energy of an isolated hydrogen atom is  $-0.5$ . The interaction energy is  $\Phi = E_0 + 0.5$ .

The boundary condition eq. (2.12) is the device by which effects of the

exchange-overlap repulsion of the adatom and metallic electrons are included in the model.

The interaction energy for an excited-state hydrogen atom is obtained by solving eqs. (2.8)–(2.12) for an excited state of the system and then subtracting the corresponding excited state energy for the isolated hydrogen atom.

The dipole moment operator for the adatom charge distribution is defined to be

$$\mu_z = L - z = -\xi. \quad (2.13)$$

A positive expectation value for  $\mu_z$  denotes a state in which the dipole is directed away from the substrate.

The quadrupole moment tensor of a distribution of charge density  $\rho(\mathbf{x})$  is [14,15], in Cartesian coordinates,

$$Q_{ij} = \int (3x_i x_j - r^2 \delta_{ij}) \rho(\mathbf{x}) d\mathbf{x}. \quad (2.14)$$

The charge distribution for the hydrogen atom–metal system has a net dipole moment so that it is necessary [14] to specify that the origin of the coordinates we use in evaluating  $Q_{ij}$  with eq. (2.14) is at the proton. For the adatom–substrate geometry here, the ground-state expectation value of  $Q_{ij}$  is diagonal in a coordinate system with  $z$  axis along our  $z$  axis and  $x$  and  $y$  axes in the plane parallel to the surface. The nonvanishing terms in the expectation values are

$$Q_{zz} = -2Q_{xx} = -2Q_{yy} = Q = -(\psi_0, (3\xi^2 - r^2) \psi_0) / (\psi_0, \psi_0). \quad (2.15)$$

The polarizability of the system is also a tensor which is diagonal in the same coordinate system which makes  $Q_{ij}$  diagonal. The independent components  $\alpha_{zz}$  and  $\alpha_{xx}$  can be defined [16,17] in terms of a second-order perturbation theory energy using a complete set of eigenstates  $\psi_n$  and energies  $E_n$  of the Hamiltonian  $H$ :

$$\alpha_{zz} = -2 \sum_{n \neq 0} |(\psi_n, \xi \psi_0)|^2 / (E_0 - E_n), \quad \alpha_{xx} = -2 \sum_{n \neq 0} |(\psi_n, x \psi_0)|^2 / (E_0 - E_n). \quad (2.16)$$

The evaluation of  $\alpha_{zz}$  and  $\alpha_{xx}$  by methods which approximate these expressions [16,17] is discussed further in section 8.

### 2.3. The assumptions

We give here a preliminary discussion of the extent to which the simplifications made in constructing the model, eqs. (2.8) to (2.12), give an inaccurate representation of the conditions obtaining in ordinary physical adsorption.

The use of perfect imaging for the evaluation of the interaction of the adatom charges with the substrate would be accurate if the metal responded instantaneously to changes in the electric field during the motion of the atomic electron. This limiting behavior of the response is approached for a metal with a high plasma frequency, i.e., high compared to the characteristic frequencies of the adatom [7,

18–20]. In a jellium model for the metal, this is fulfilled for a metal of high electron density.

We use a sharp, nondiffuse, metallic surface as the boundary for the accessible space of the adatom electron. In fact the substrate electrons spill out past the ion cores, with the density dropping to nearly zero over a distance of the order of a few  $a_0$ . Model calculations show the spillout distance becomes small for a high density metal [19,21].

The response of the substrate is characterized by a dielectric constant, which is a concept of linear response of the substrate to an external field. At small charge–substrate separations, the strong electric field of the charge may drive a significantly nonlinear response [6]. The substrate is treated as a continuum, with no allowance for effects of its discrete atomic structure [18].

These complications place a lower limit on the charge–surface separations for which the use of electrostatic image potentials is physically accurate [5,6]. Phenomena calculated with our model which depend appreciably on small charge–surface separations must be treated with reservations.

The assumption that the atomic electron is excluded from the interior of the substrate will reflect the physical situation if the work function of the substrate is appreciably smaller than the ionization potential of the adatom [3]. This assumption appears likely to be more accurate for the ground state of the system than for the excited states. Our use of this assumption is an essential ingredient of the model and we do not see a way to begin a systematic approximation method which improves upon it and retains the one-electron nature of the model.

### 3. Qualitative features of the interaction energy

The ground state interaction energy  $\Phi$  is defined to be the difference between the ground state energy  $E_0$  of eq. (2.8) and the ground state energy of an isolated hydrogen atom ( $-1/2$ ). Here, in section 3.1, we show that the limiting behaviors of  $\Phi$  at large and small separations can be established by inspection: at large separations  $\Phi$  is negative and at small separations ( $L \rightarrow 0$ ),  $\Phi$  is unboundedly negative ( $\Phi \rightarrow -\infty$ ). Thus there is a question whether a local minimum in  $\Phi$  is formed for the model. In section 3.2 we establish that there is a region of positive  $\Phi$ , and therefore that a local minimum is formed, by construction of a positive lower bound on  $\Phi$  at some separations. The interaction energy in excited states of the atom does not necessarily have a local minimum, as shown by detailed results in section 6.3.2.

#### 3.1. The limits of large and small $L$

The model in eqs. (2.8) to (2.11), without the specification of eq. (2.12), was used by Lennard-Jones [1] to estimate the interaction energy of a hydrogen atom with a metal. His treatment, a perturbation theory at large  $L$ , gives the result [1]

$$\Phi \simeq -1/(4L^3), \quad L \rightarrow \infty. \quad (3.1)$$

The physical picture is that in this limit the system decouples into an isolated atom plus metal, with a small lowering of the total energy coming from the interaction of the fluctuating dipole moment on the atom with its image in the metal. Eq. (3.1) is discussed further in section 4.1.

At small separations, the simplifications made in constructing the Hamiltonian become suspect [5,6]. Nevertheless, we discuss this limiting case to establish the qualitative content of the model. The potential  $V$  can be viewed as the energy of the proton and its image plus the energy of the electron and its image plus the energy of the electron in the field of a finite dipole formed from the proton and the image proton. At small  $L$  the dipole becomes small and the electron energy is dominated by its binding to its image, with an energy  $-1/32$ . Then the interaction energy is dominated by the proton–image proton energy:

$$\Phi \simeq -1/(4L), \quad L \rightarrow 0. \quad (3.2)$$

Eqs. (3.1) and (3.2) are consistent with many possible variations of  $\Phi$  at intermediate separations. Our intent in constructing the model was that a minimum in  $\Phi$  would be formed by a balance between the attractive polarization potential, indicated in eq. (3.1), and an effective repulsion of the atomic electron from the metal, incorporated in eq. (2.12). The arguments leading to eq. (3.2) fail for physical systems because image potentials are not to be used so literally at small  $L$ . We now investigate whether this failure influences the model so much that no finite potential minimum is formed.

### 3.2. Potential barrier at intermediate separations

The results of a Rayleigh–Ritz variational calculation of the ground state energy of eq. (2.8), presented in sections 5 and 6, show that there is indeed a region of positive  $\Phi$  between the large and small  $L$  regions discussed in section 3.1. In practice there are questions about the effective convergence of variational calculations with finite basis sets, so that we believe it is appropriate to give a further proof of the existence of the potential barrier for this model.

The technical difficulty we encounter in solving eq. (2.8) is that we do not know of a coordinate system in which the variables separate [6]. Even for the ground state, with cylindrical symmetry about the  $z$  axis, the Schrödinger equation remains a partial differential equation in two variables. We now construct a comparison problem with separable Hamiltonians for which the equations to be solved are ordinary second order differential equations and which leads to a lower bound on  $E_0$  and  $\Phi$ .

Rewrite the Schrödinger equation as

$$[E_0 + 1/(4L)] \psi_0 = (H_i + H_d) \psi_0, \quad (3.3)$$

with

$$H_i = (1 - \lambda)K - 1/(4z), \quad (3.4)$$

and

$$H_d = \lambda K + [\rho^2 + (z + L)^2]^{-1/2} - [\rho^2 + (z - L)^2]^{-1/2}, \quad (3.5)$$

subject to

$$\psi_0 = 0, \quad z = 0. \quad (3.6)$$

The separation of  $K$  between eqs. (3.4) and (3.5) is made with a quantity  $\lambda$  ( $0 < \lambda < 1$ ) which is available as a variational parameter. The Hamiltonian  $H_i$  describes the interaction of a charge with its image [22,23] and  $H_d$  describes the interaction of a charge with a finite dipole [24].

The lower bound on  $E_0$  results from the observation that  $E_0 + 1/(4L)$  must be greater than or equal to the sum of the ground state energies of  $H_i$  and  $H_d$ , each subject to eq. (3.6):

$$E_0(H) \geq -(1/4L) + E_0(H_i) + E_0(H_d). \quad (3.7)$$

The ground state energy of  $H_i$  is available analytically:

$$E_0(H_i) = -1/[32(1 - \lambda)]. \quad (3.8)$$

The ground state energy of  $H_d$  is obtained by an analysis similar to that of Wallis et al. [24] for the energy levels of a finite-dipole potential. The Schrödinger equation separates in the confocal elliptic coordinates of section 2.1: the  $\xi$  equation is the same equation as treated by Wallis et al.; the  $\eta$  equation is formally the same as theirs but the plane  $z = 0$  is not a symmetry plane of  $V$  so that the boundary condition at  $z = 0$  ( $\eta = 0$ ) prevents us from making direct use of their results. We solved for the ground state energy with our boundary condition by numerical integration of the separated equations to get a pair of simultaneous equations for the separation constant in terms of the energy. Our results for the  $\xi$  equation agree with those of Wallis et al. [24]. We obtain, numerically, the ground state energy in the form

$$E_0(H_d) = -(\lambda/2L^2) p^2(4L/\lambda), \quad (3.9)$$

where  $p^2$  is a reduced energy which depends on the combination  $4L/\lambda$ .

The function  $p^2$  arises in expressing the Schrödinger equation in reduced units; it is a nonnegative increasing function of its argument.

Because there is no binding for  $H_d$ , with eq. (3.6), for values [25] of  $4L/\lambda$  less than 2.958, we have a lower bound on  $\Phi$  at small  $L$  with the same leading terms as shown in eq. (3.2).

The lower bound, eq. (3.7), is

$$E_0 \geq E_{1b} = -1/(4L) - 1/[32(1 - \lambda)] - (\lambda/2L^2) p^2(4L/\lambda), \quad (3.10)$$

and we may choose the parameter  $\lambda$  to make the rhs a maximum for a given value



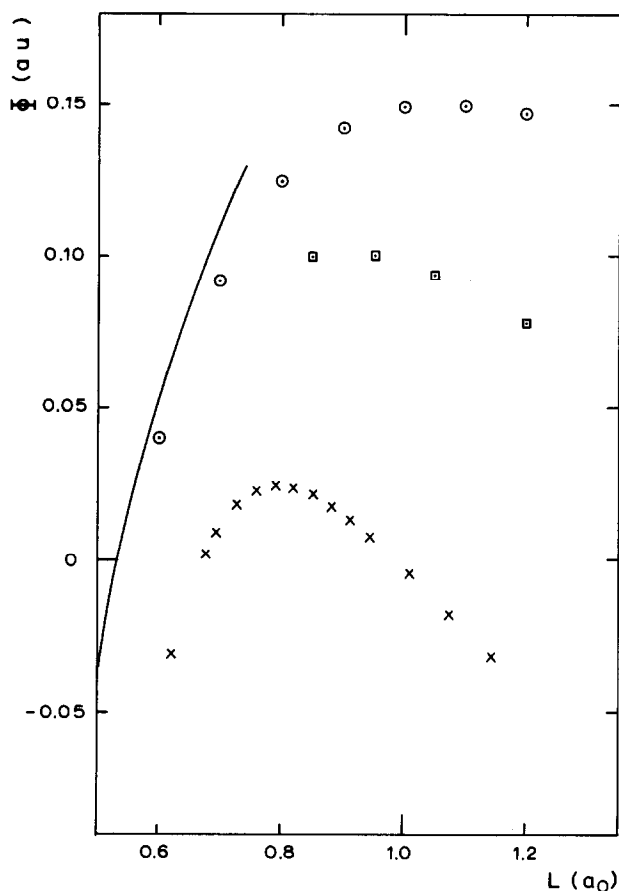


Fig. 2. Potential barrier at intermediate separation. Upper and lower bounds on the ground-state interaction energy  $\Phi$  are shown as a function of proton distance  $L$  from the surface (entries are in atomic units): (x) lower bound calculated as described in section 3.2; (o) upper bound calculated as described in section 5; (□) upper bound calculated as described in section 6.1; solid line: upper bound calculated from eq. (3.11).

of  $L$ . Actually there are more convenient procedures, based on the fact that the function  $p^2$  is calculated at discrete values of its argument, but the principle remains the same: we maximize the lower bound.

The resulting lower bound on  $\Phi$  is shown in fig. 2: it proves that there is a region of positive  $\Phi$  which includes the range of  $L$  from 0.7 to  $0.95 a_0$ . There is a potential barrier in  $\Phi$  of height at least equal to 0.024 au. Because a lower bound based on arguments such as those leading to eq. (3.7) is frequently a poor approximation to the exact energy we may expect that the barrier is much higher than the estimate gives. Our detailed calculations show it to be approximately 0.1 au.

The lower bound construction we have just presented differs from many application of such arguments in not working solely with analytical results, so that it is not simple to reproduce the results we have used. However, the comparison problem for  $H_d$  can be treated with much higher precision than the problem for  $H$ , so that the resort to numerical methods in the lower bound remains of value. A conservative statement of the situation is that use of the lower bound to establish the barrier is a calculation with a very different computational bias than the variational calculations on which we base most of our discussion.

### 3.3. Further estimates of the interaction

We obtain an upper bound on the interaction  $\Phi$  without detailed calculation by the observation that the potential in  $H_d$ , eq. (3.5), is negative in the half-space  $z > 0$ :

$$\Phi \leq (15/32) - 1/(4L). \quad (3.11)$$

This upper bound is shown in fig. 2 Eq. (3.11) and the argument below eq. (3.9) confirm the estimate given in eq. (3.2).

The importance of the wall boundary condition for the existence of the barrier in  $\Phi$  can be seen from the following arguments which overlook the boundary condition.

First, rewrite the image potential  $V_i$  in eq. (2.11) with cylindrical coordinates centered on the proton:

$$V_i = -1/(4L) - 1/[4(\xi + L)] + [\rho^2 + (\xi + 2L)^2]^{-1/2}, \quad -L < \xi < \infty. \quad (3.12)$$

The image potential  $V_i$  is negative throughout the half-space  $z < 0$  ( $\xi > -L$ ), and thus is a negative definite perturbation on the isolated atom Hamiltonian. Because of the boundary condition eq. (2.12) we must not conclude that  $E_0$  is always less than the energy of the isolated hydrogen atom.

Similarly, although we can show that

$$\partial V_i / \partial L|_{\xi, \rho} \geq 0, \quad \xi \geq -L, \quad (3.13)$$

we must not use the Hellman–Feynman theorem [13,26] to conclude that the ground state energy  $E_0$  is monotonic function of  $L$ .

Both conclusions would be false, as is shown by the results of sections 3.2, 5 and 6.

## 4. Perturbation theory results

Our model has been analyzed for large proton-surface separations  $L$  by Lennard-Jones [1] and by Antoniewicz [2], using perturbation theory. In their calculations, the condition on the atomic electron wave function in the region of the metal, our

eq. (2.12), is not stated explicitly. Specifying the substrate response with image potentials reduces the complexity of the calculations [11] so that the polarization of Lennard-Jones arises in the first order of perturbation theory for the energy and the dipole moment of Antoniewicz is obtained with first-order perturbation theory for the wave function.

In this section we review and refine the perturbation theory results [27]. In later sections they are used as guides in deciding how complex a variational trial function is needed to represent the leading multipole distortions of the adatom-electron density and for quantitative analysis of the results of the variational calculations at large  $L$ .

The basic Hamiltonian in the perturbation theory is the Hamiltonian for an isolated hydrogen atom:

$$H_0 = -\frac{1}{2}\nabla^2 - 1/r. \quad (4.1)$$

The image interactions,  $V_i$  in eq. (2.11) provide the perturbing potential. At large  $L$  (and finite  $r$ ),  $V_i$  is expanded to form a series:

$$V_i = (1/L^3) V_3 + (1/L^4) V_4 + (1/L^5) V_5 + \dots, \quad (4.2)$$

with

$$V_3 = -(\xi^2 + r^2)/16, \quad (4.3)$$

$$V_4 = \xi(\xi^2 + r^2)/16, \quad (4.4)$$

$$V_5 = (3/256) r^4 - (15/128) r^2 \xi^2 - (29/256) \xi^4. \quad (4.5)$$

#### 4.1. The interaction energy

The ground-state energy of  $H_0$ ,  $E_0^{(0)}$ , is  $-1/2$ , with a normalized wave function

$$\phi_0 = \pi^{-1/2} \exp(-r). \quad (4.6)$$

First order perturbation theory for the ground-state energy [1] shows the leading term in the interaction energy  $\Phi$  to be the expectation value of  $V_i$  in the state  $\phi_0$ :

$$\Phi^{(1)} = (\phi_0, V_i \phi_0) / (\phi_0, \phi_0). \quad (4.7)$$

A calculation with eqs. (4.3) to (4.5) gives

$$\Phi^{(1)} = -1/(4L^3) - 9/(8L^5) - \dots. \quad (4.8)$$

The second order of perturbation theory for  $\Phi$  is discussed in section 4.4.

Similar constructions hold for the interaction energy of the excited state atom. We list here results for states formed from the degenerate first excited state of the hydrogen atom. The interaction energy then is the difference between the excited state energies of eq. (2.8) and the energy  $[-(1/8)]$  of the isolated atom. The first excited state of the isolated atom (principal quantum number  $n = 2$ ) [28] is 4-fold

degenerate, but in interaction with the metal the degeneracy is partially lifted. The  $2p, m = \pm 1$  states remain degenerate (polar axis perpendicular to the metal), but the  $2s$  and the  $2p, m = 0$  states split from these.

Perturbation theory for the  $2p, |m| = 1$  states follows the calculation with eq. (4.7). The result is

$$\Phi^{(1)}(2p, |m| = 1) \simeq -9/(4L^3). \quad (4.9)$$

Perturbation theory for the  $2s$  and  $2p, m = 0$  states must include the fact that they are mixed by the  $V_4$  part of the perturbation, which is odd in  $\zeta$ . Applying degenerate perturbation theory gives the results

$$\begin{aligned} \Phi^{(1)}(2p) &\simeq [1/(4L^3)] \{-13 + [1 + (90/L)^2]^{1/2}\}, \\ \Phi^{(1)}(2s) &\simeq [1/(4L^3)] \{-13 - [1 + (90/L)^2]^{1/2}\}. \end{aligned} \quad (4.10)$$

The labelling of these interactions is based on analysis of the perturbed wave functions at very large  $L$ ; at values of  $L$  near 5, however, the unperturbed  $2s$  and  $2p, m = 0$  states are nearly equally mixed.

#### 4.2. The dipole moment

The average dipole moment of the system lies along the  $z$  axis and is given by the expectation value of the dipole moment operator, eq. (2.13) in the ground state:

$$\mu = (\psi_0, \mu_z \psi_0) / (\psi_0, \psi_0). \quad (4.11)$$

Perturbation theory leads to a series for the wave function

$$\psi_0 = \phi_0 + \psi^{(1)} + \dots, \quad (4.12)$$

with

$$\psi^{(1)} = \left[ \frac{1 - P_0}{E_0^{(0)} - H_0} \right] V_1 \phi_0. \quad (4.13)$$

The factor  $1 - P_0$  is a projection operator to enforce that  $\psi^{(1)}$  is orthogonal to  $\phi_0$ .

The leading term in the dipole moment at large  $L$  is [2]

$$\mu^{(1)} = 2(\phi_0, \mu_z \psi^{(1)}). \quad (4.14)$$

Of the terms shown in eqs. (4.2) to (4.5), only  $V_4$  gives a nonvanishing contribution to  $\mu^{(1)}$ . We evaluate this in two ways. First, we note that there is a closed form solution [29] for the first order Stark-perturbed wave function of a hydrogen atom:

$$\left[ \frac{1 - P_0}{E_0^{(0)} - H_0} \right] \zeta \phi_0 = -\zeta [1 + (r/2)] \phi_0. \quad (4.15)$$

The self-adjointness of the resolvent operator in eq. (4.13) can be used to bring eq.

(4.14) to a form where eq. (4.15) is used; the result is

$$\mu^{(1)} = (99/16)(1/L^4) + \dots \quad (4.16)$$

Second, the same methods [29] which lead to eq. (4.15) are used to find a closed form for the part of  $\psi^{(1)}(V_4)$  which gives a nonvanishing contribution to eq. (4.14)

$$\frac{1 - P_0}{E_0^{(0)} - H_0} \left( \frac{3}{20} \zeta r^2 \right) \phi_0 = -\zeta [(3/80)r^3 + (9/80)r^2 + (9/32)r + (9/16)] \phi_0. \quad (4.17)$$

Eq. (4.17) is the dipole contribution of  $V_4$  in  $\psi^{(1)}$ ;  $V_4$  also gives an octupole contribution to  $\psi^{(1)}$ . Using eq. (4.17) in eq. (4.14) again leads to eq. (4.14).

Eq. (4.16) is a slight improvement on the result of Antoniewicz [2], who approximated the evaluation of the coefficient of  $(1/L^4)$ .

The next term in  $\mu^{(1)}$  arises from the  $V_6$  term in eq. (4.2), not shown explicitly there. Its contribution is easily found using eq. (4.15):

$$\mu^{(1)} \simeq (99/16)(1/L^4) + (585/8)(1/L^6). \quad (4.18)$$

This series does not appear to converge rapidly, even at  $L$  near 5.

### 4.3. The quadrupole moment

The quadrupole moment tensor is defined and discussed at eqs. (2.14) and (2.15), where it is given in terms of a single expectation value  $Q$ .

Using eq. (4.12), the leading term in  $Q$  at large  $L$  is

$$Q^{(1)} = -2(\phi_0, [3\zeta^2 - r^2] \psi^{(1)}). \quad (4.19)$$

The leading contribution to  $Q^{(1)}$  comes from  $V_3$ . The quadrupole perturbation in  $\psi^{(1)}$  from  $V_3$  is

$$\frac{1 - P_0}{E_0^{(0)} - H_0} [-(1/48)(3\zeta^2 - r^2) \phi_0] = (1/96)[1 + (2r/3)](3\zeta^2 - r^2) \phi_0. \quad (4.20)$$

Thus the leading term in  $Q^{(1)}$  is

$$Q^{(1)} = -(5/4L^3). \quad (4.21)$$

An extended calculation using eq. (4.15) and  $V_5$  leads to a second term:

$$Q^{(1)} \simeq -(5/4L^3) - (72/L^5). \quad (4.22)$$

### 4.4. Second-order perturbation theory for $\Phi$

We have shown the leading dipole and quadrupole contributions to the first-order perturbed wave function  $\psi^{(1)}$  in eqs. (4.17) and (4.20). The derivation of these terms is quite similar to the derivation [29] of the first-order Stark term, eq.

(4.15). To complete the calculation of the leading term in the second-order energy  $\Phi^{(2)}$ , which varies as  $1/L^6$ , we now evaluate the contribution of the spherically symmetric portion of  $V_3$  to  $\psi^{(1)}$ . There is a slight complication in the evaluation of this piece, which we denote  $\psi_0^{(1)}$ . Therefore we include an outline of it.

The equation determining  $\psi_0^{(1)}$  is

$$-\left(\frac{1}{12L^3}\right)\left[\frac{1-P_0}{E_0-H_0}\right]r^2\phi_0=\psi_0^{(1)}. \quad (4.23)$$

If we define a function  $f_0$  by

$$\psi_0^{(1)} \equiv -1/(6L^3)f_0(r)\phi_0, \quad (4.24)$$

eq. (4.23) can be written as a differential equation for  $f_0$ :

$$2(E_0-H_0)f_0\phi_0=[1-P_0]r^2\phi_0=(r^2-3)\phi_0, \quad (4.25)$$

where the last equality is a consequence of the orthogonality imposed by the projection operator  $P_0$ . Explicitly the differential equation for  $f_0$  is

$$d^2f_0/dr^2 + [(2/r) - 2] df_0/dr = r^2 - 3. \quad (4.26)$$

The solution, with an additive term determined by the requirement that  $\psi_0^{(1)}$  is orthogonal to  $\phi_0$ , is

$$f_0 = -(1/6)r^3 - (1/2)r^2 + (11/4). \quad (4.27)$$

As in the calculations with differential equations [29] leading to eqs. (4.15), (4.17), and (4.20), there is a singular solution to the homogeneous version of eq. (4.25). It is rejected because of an implicit condition that the first order perturbed wave function is nonsingular.

The leading term in the second-order energy is evaluated using eqs. (4.27) and (4.20):

$$\Phi^{(2)} = (\phi_0, V_1\psi^{(1)}) \simeq -(91/384)(1/L^6). \quad (4.28)$$

## 5. Variational calculation at small separations

At small separations  $L$ , the discussion of section 3 shows that the binding of the electron to its image is the dominant process and that the lateral ( $\rho$  coordinate) localization is rather weakly enforced by the interaction of the electron with the finite dipole of the proton and image proton. This picture is now incorporated in a variational trial function for the ground-state energy which reflects these effects already in its nonoptimized form. Inspection of the results shows that the picture becomes accurate only for values of  $L$  which are much smaller than those which are significant for the physical holding potential.

Specifically, we adopt a trial function

$$\psi_t = z \exp(-\alpha z) R(\rho), \quad (5.1)$$

where  $\alpha$  is a variational parameter and  $R(\rho)$  is a function to be determined by minimizing the Rayleigh–Ritz trial energy. The choice  $\alpha = 1/4$  makes the  $z$ -dependence exactly that of the electron–electron image ground state wave function. The functional variation of the trial energy with respect to  $R(\rho)$  leads to a Schrödinger equation for planar motion in a purely attractive potential which is formed by averaging the potential  $V$ , eq. (2.11), with the  $z$  density. For any finite  $L$  there is a bound-state, square-integrable, solution [30] for  $R(\rho)$ . Thus the trial energy obtained in this way is a tighter upper bound than is given in eq. (3.11).

The upper bound resulting from the use of eq. (5.1) is shown in fig. 2. The evaluation of the effective potential in the Schrödinger equation for  $R(\rho)$  and the solution for  $R(\rho)$  were done by numerical integration for several values of  $\alpha$  at given  $L$ .

To measure the extent to which the picture of the dominant process being the electron binding to its image is confirmed by these calculations, we compare the electron trial energy,  $E_t + 1/(4L)$ , with the ground state energy  $-1/32 = -0.03125$  of the electron-image system. At  $L = 1.0$ , the electron trial energy is  $-0.101$  and at  $L = 0.6$  it is  $-0.0432$ ; the optimal values of  $\alpha$  at these separations are 0.614 and 0.347 respectively.

We conclude that the picture is accurate only for values of  $L$  much smaller than 1. The considerations for choosing eq. (5.1) as a trial function are much less compelling at values of  $L$  greater than 1; indeed the corresponding trial energy is a noticeably poorer upper bound than we obtain in section 6.

The results obtained here with eq. (5.1) establish the small- $L$  limit for a large-scale variational calculation, while the perturbation theory results establish the large- $L$  limit.

## 6. Detailed treatment of the model: multiparameter variational calculation

To get accurate solutions at intermediate distances  $L$  for the interaction energy  $\Phi$  and the dipole moment  $\mu$  and the quadrupole moment  $Q$  of the atomic charge distribution, we resort to a variational solution for the ground state of the model stated in eqs. (2.8) to (2.12). The values we give for  $\Phi$  are in fact upper bounds to the exact  $\Phi$ , but we conclude from the stability of our values for  $\Phi$ ,  $\mu$ , and  $Q$  as the scope of the variational search is expanded that we have essentially obtained the exact values of these quantities for the model.

This section also contains results for the first excited states of the model, corresponding to the  $n = 2$  states of an isolated hydrogen atom, and results for the ground state of a model obtained from eqs. (2.8) to (2.12) by omission of  $V_i$  from the potential. The latter model is the case of hydrogen atom in the presence of an impenetrable wall (“no images”).

### 6.1. Trial functions and pattern of calculation – ground state

The trial function which we use for the ground-state calculations has the form

$$\psi_t = \exp(-\alpha\xi/2) \sinh(\beta\eta/2) \sum_{k,l} C_{kl} \xi^k \eta^l, \quad (6.1)$$

in the confocal elliptic coordinates [13] of section 2.1. It has two nonlinear parameters  $\alpha$  and  $\beta$  and up to 28 linear parameters  $C_{kl}$ . There are several advantages to the use of this form of the trial function.

The volume integral in the trial energy and the expectation values for  $\mu$  and  $Q$  reduce to combinations of the integrals

$$I_n(\alpha) = \int_1^\infty \xi^{n-1} e^{-\alpha\xi} d\xi, \\ J_n(\beta) = \int_0^1 \eta^{n-1} \sinh^2(\beta\eta/2) d\eta. \quad (6.2)$$

Except for the case  $n = 0$  these can be given in terms of elementary functions; for  $n = 0$  the evaluation is simplified by using tabulated values [31] of exponential integrals as reference points for numerical integrations. Thus most of the reduction of the integrations is performed analytically.

Second, at large  $L$  the function  $\psi_t$  closely approximates the ground-state wave function of an isolated hydrogen atom when only the  $k = l = 0$  term is retained in the sum and the nonlinear parameters are chosen to be  $\alpha = \beta = 2L$ . The trial energy then has the leading  $1/L^3$  term of the perturbation theory [1], eq. (4.8).

Third, we find that for values of  $L$  in the range 1 to 6 the minimized trial energy with 28 linear parameters differs by less than  $\frac{1}{2}\%$  from the value obtained with only the  $k = l = 0$  term if  $\alpha$  and  $\beta$  are chosen to minimize the 1-term trial energy. The values for  $\mu$  and  $Q$  also appear to go rapidly to limiting values as the number of linear parameters is increased; the values ordinarily change by less than 1% as the number of linear parameters is increased from 10 to 28.

The principal disadvantage of the trial function eq. (6.1) is that the separate powers do not form an orthogonal basis in the half-space  $z > 0$ . An overlap matrix,

$$S(kl|k'l') \equiv \int_0^1 d\eta \int_1^\infty d\xi (\xi^2 - \eta^2) \xi^{k+k'} \eta^{l+l'} e^{-\alpha\xi} \sinh^2(\beta\eta/2), \quad (6.3)$$

appears in the linear variational problem for the coefficients  $C_{kl}$ . The matrix eigenvalue problem for the  $C_{kl}$ 's is first reduced to a more standard eigenvalue problem by applying a Cholesky decomposition [32] to the overlap matrix. This step, particularly at small  $L$ , is sensitive to lack of precision in the evaluation of the elements of the overlap matrix. It is not routine to extend the calculations beyond 28 linear parameters with our methods.



Our procedure for increasing the number of variational parameters in (6.1) is to include all terms in the sum ( $k$  and  $l$  are nonnegative integers) satisfying

$$k + l \leq N$$

for successive values of  $N$ . We use  $N$  values of 0 to 6, or a range from 1 to 28 terms in the sum. The powers of the coordinates shown in the first-order perturbed wave functions in eqs. (4.17) and (4.20) are included in the trial function when  $N$  is greater than or equal to 5. However, as in other applications of variational methods, we find our values for  $\mu$  and  $Q$  are already near their apparent limits at  $N$  equal to 3 or 4.

In outline, the steps of the variational calculation for the ground state are, at each  $L$ : (1) For a 1-term trial function, with  $k = l = 0$ , we determine the values of  $\alpha$  and  $\beta$  (to 1%) which minimize the trial energy. (2) The values of  $\alpha$  and  $\beta$  are held fixed and the minimum trial energy is found for values of  $N$  up to 6, using library routines of our computer center for the Cholesky decomposition and the determination of matrix eigenvalues. (3) The optimized trial function is used instead of the exact ground-state function to calculate  $\mu$  and  $Q$  from eqs. (2.15) and (4.11). (4) At scattered values of  $L$  the effect of varying  $\alpha$  and  $\beta$  in the  $N = 6$  case is checked to see if they need to be reoptimized; in all cases we have found the changes in  $\Phi$ ,  $\mu$ , and  $Q$  to be negligible compared to the precision with which our results are reported.

At large and small  $L$  values the overlap matrix has some very small eigenvalues for the optimized  $\alpha$  and  $\beta$  and values of  $N$  greater than 3. This led, at times, to instability in the  $N = 6$  calculations; for such cases our reported results were obtained as limits inferred from the 3, 4, and 5 values and were checked with limits derived from the  $N = 6$  case with a small stabilizing component added to the overlap matrix.

We believe the results we obtain for the energy  $E_0 (= -0.5 + \Phi)$  are accurate to 6 figures and for  $\mu$  and  $Q$  are accurate to 3 figures.

## 6.2. Trial functions and pattern of calculation-excited states

Variational principles are available for the interaction energy of the excited-state atom [32,33].

For the degenerate states formed from the  $2p$ ,  $m = \pm 1$  states of the isolated atom (discussed in section 4.1), we use a variational trial function

$$\tilde{\Psi} = \exp(\pm i\phi) [(\xi^2 - 1)(1 - \eta^2)]^{1/2} \exp(-\alpha'\xi/2) \sinh(\beta'\eta/2) \sum_{k,l} d_{kl} \xi^k \eta^l, \quad (6.4)$$

and determine the minimum trial energy, following the same pattern of calculation described in section 6.1. However, the search for the optimal values of  $\alpha'$  and  $\beta'$  in the  $N = 0$  case is less thorough, because of the insensitivity of the  $N = 5$  results to the precise values taken for  $\alpha'$  and  $\beta'$ . Most of the results which we report for the

excited states are obtained with the  $N = 5$  trial function.

The  $\phi$ -dependence assures that this trial function is orthogonal to the ground-state function, so that the usual Rayleigh–Ritz procedure leads to an upper bound on the interaction energy in these excited states. The stability of the trial energy as the number of linear variational parameters is increased gives us confidence that we have evaluated the interaction energy to within  $2 \times 10^{-4}$  au.

The interaction energies for the other two  $n = 2$  states, formed from the 2s and 2p,  $m = 0$  states of the isolated atom, are obtained from the results for the trial function of section 6.1. These states are independent of  $\phi$ . Upper bounds on the interaction energies in the excited states are derived from the diagonalization of the (truncated) trial Hamiltonian matrix. The lowest eigenvalue of the linear variational problem is an upper bound on the ground-state energy; the next two eigenvalues are upper bounds on the energies of the first and second excited states [32,33]. For each eigenvalue we vary the nonlinear parameters  $\alpha$  and  $\beta$  to obtain the best upper

Table 1  
Properties of the ground state of the hydrogen atom – imaging substrate system <sup>a</sup>

$L^b$	$\Phi^c$	$\mu^d$	$Q^e$
0.85	$9.98 \times 10^{-2}$	-1.605	-3.30
0.95	0.1001	-1.253	-1.94
1.05	$9.35 \times 10^{-2}$	-1.010	-1.14
1.2	$7.788 \times 10^{-2}$	-0.767	-0.471
1.6	$3.757 \times 10^{-2}$	-0.428	+0.158
2.0	$1.384 \times 10^{-2}$	-0.257	+0.302
2.4	$2.29 \times 10^{-3}$	-0.153	0.304
2.8	$-2.54 \times 10^{-3}$	$-8.59 \times 10^{-2}$	0.253
3.0	$-3.59 \times 10^{-3}$	$-6.24 \times 10^{-2}$	0.220
3.2	$-4.11 \times 10^{-3}$	$-4.38 \times 10^{-2}$	0.186
3.4	$-4.27 \times 10^{-3}$	$-2.94 \times 10^{-2}$	0.154
3.6	$-4.21 \times 10^{-3}$	$-1.85 \times 10^{-2}$	0.124
3.8	$-4.02 \times 10^{-3}$	$-1.02 \times 10^{-2}$	$9.74 \times 10^{-2}$
4.0	$-3.75 \times 10^{-3}$	$-4.24 \times 10^{-3}$	$7.42 \times 10^{-2}$
4.4	$-3.14 \times 10^{-3}$	$+2.95 \times 10^{-3}$	$3.83 \times 10^{-2}$
4.8	$-2.55 \times 10^{-3}$	$+5.95 \times 10^{-3}$	$1.52 \times 10^{-2}$
5.2	$-2.05 \times 10^{-3}$	$6.66 \times 10^{-3}$	$1.50 \times 10^{-3}$
5.6	$-1.65 \times 10^{-3}$	$6.23 \times 10^{-3}$	$-5.57 \times 10^{-3}$
6.0	$-1.34 \times 10^{-3}$	$5.46 \times 10^{-3}$	$-8.57 \times 10^{-3}$
6.4	$-1.09 \times 10^{-3}$	$4.54 \times 10^{-3}$	$-9.23 \times 10^{-3}$
6.8	$-8.96 \times 10^{-4}$	$3.70 \times 10^{-3}$	$-8.78 \times 10^{-3}$

<sup>a</sup> All entries in atomic units: 1 hartree  $\simeq 27.21$  eV,  $1a_0 \simeq 0.5292$  Å,  $1ea_0 \simeq 2.542 \times 10^{-18}$  esu-cm = 2.542 debye,  $1ea_0^2 \simeq 1.345 \times 10^{-26}$  esu-cm<sup>2</sup>.

<sup>b</sup> Perpendicular distance of proton to surface.

<sup>c</sup> Interaction energy,  $\Phi = E_0 + 0.5$ .

<sup>d</sup> Dipole moment, eq. (4.11); positive  $\mu$  denotes an outward directed dipole.

<sup>e</sup> Quadrupole moment, eq. (2.15).

bounds on the energies of the ground and first and second excited states of azimuthal symmetry with the trial function eq. (6.1).

The convergence of the variational approximation with increasing basis size is less rapid for the excited states than for the ground state. Also, the problems of numerical stability mentioned in section 6.1 become more severe in the excited states. We believe our results for the energies of the excited states of azimuthal quantum number  $m = 0$  are accurate to within  $2 \times 10^{-4}$  au.

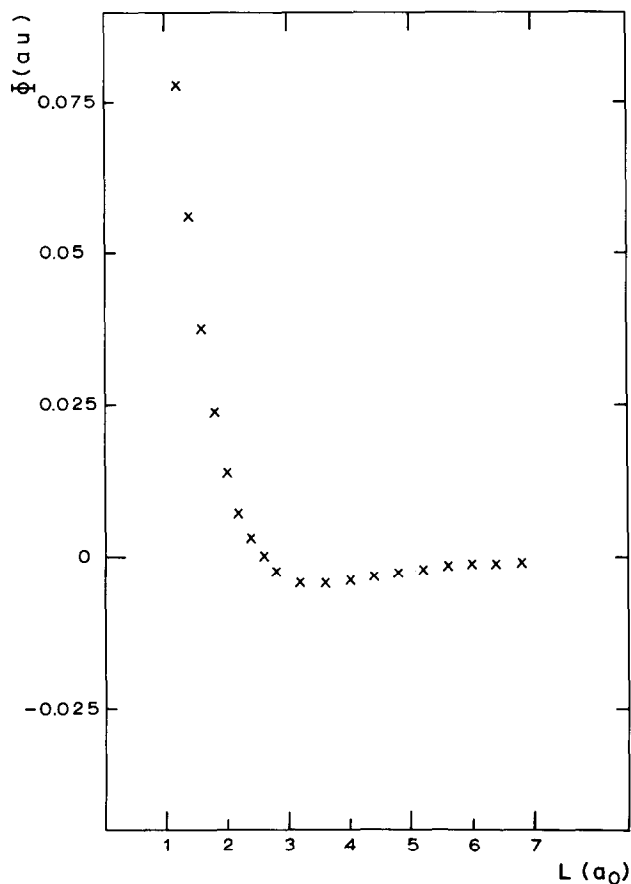


Fig. 3. Interaction energy of a ground state hydrogen atom and perfectly imaging wall. The energy  $\Phi$  is shown as a function of proton distance  $L$  from the wall (entries are in atomic units). The points are the results of the multiparameter variational calculation described in section 6.1; the data are also presented in table 1.

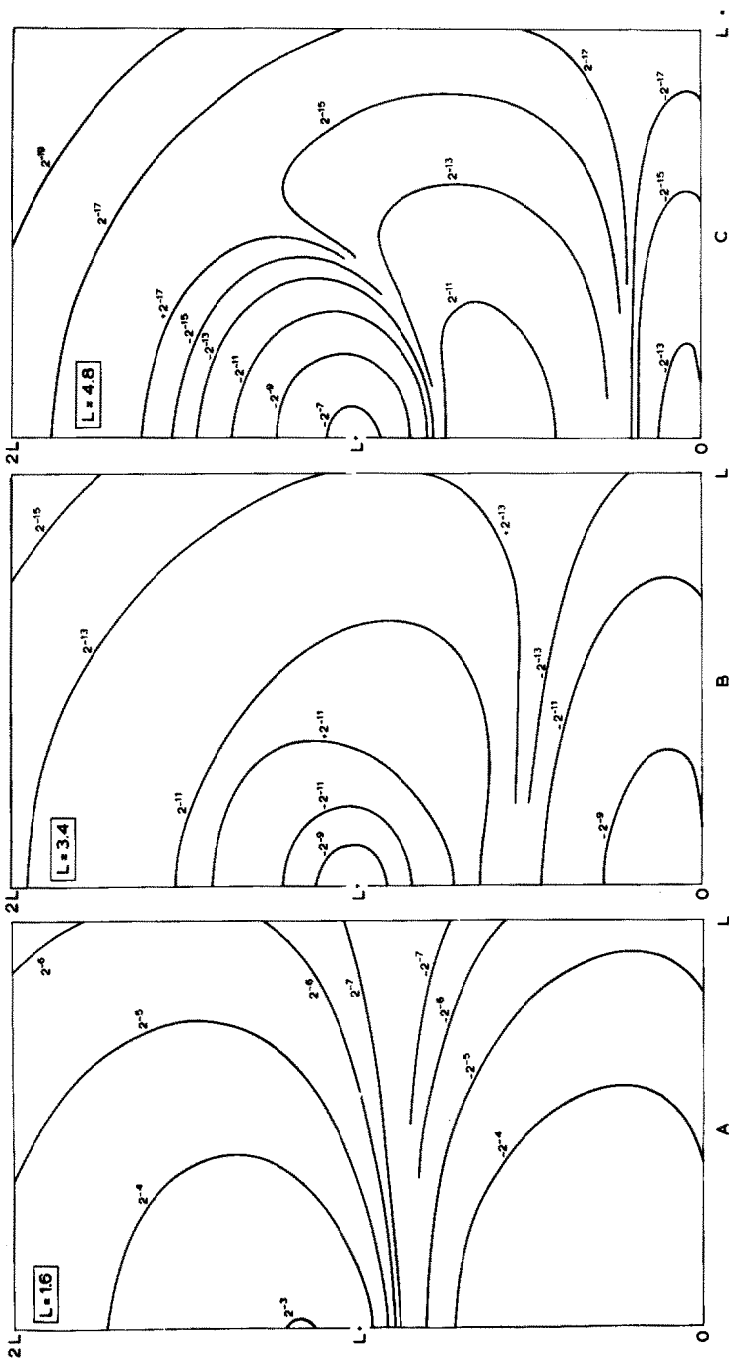


Fig. 4. Contours of constant density deviation. Contours are shown for constants values of  $|\psi_0|^2 - 2e^{-2r}$ , for the change in the probability density of the atomic electron relative to the isolated atom probability density (both densities are normalized to  $8\pi$ ). See discussion in section 6.3 of the text. The ordinate is the distance  $z$  from the surface and the abscissa is the lateral distance  $\rho$  from the  $z$  axis. The proton is at distance  $L$  from the surface along the  $z$  axis: (a)  $L = 1.6$ , (b)  $L = 3.4$ , (c)  $L = 4.8$ .

Table 2

Properties of the ground state of the hydrogen atom—impenetrable wall system <sup>a</sup>

$L$	$\Phi$	$\mu$	$Q$
0.85	0.233	-1.20	-2.27
0.95	0.205	-1.02	-1.53
1.2	0.1428	-0.704	-0.54
1.6	$7.56 \times 10^{-2}$	-0.432	+0.027
2.0	$3.92 \times 10^{-2}$	-0.279	+0.201
2.4	$2.01 \times 10^{-2}$	-0.182	+0.237
2.8	$1.03 \times 10^{-2}$	-0.117	0.218
3.2	$5.21 \times 10^{-3}$	-0.074	0.177
3.6	$2.62 \times 10^{-3}$	$-4.53 \times 10^{-2}$	0.133
4.0	$1.31 \times 10^{-3}$	$-2.72 \times 10^{-2}$	$9.47 \times 10^{-2}$
4.4	$6.47 \times 10^{-4}$	$-1.60 \times 10^{-2}$	$6.42 \times 10^{-2}$
4.8	$3.18 \times 10^{-4}$	$-9.22 \times 10^{-3}$	$4.18 \times 10^{-2}$
5.2	$1.55 \times 10^{-4}$	$-5.21 \times 10^{-3}$	$2.64 \times 10^{-2}$
5.6	$7.53 \times 10^{-5}$	$-2.90 \times 10^{-3}$	$1.62 \times 10^{-2}$
6.0	$3.63 \times 10^{-5}$	$-1.59 \times 10^{-3}$	$9.73 \times 10^{-3}$
6.4	$1.74 \times 10^{-5}$	$-0.86 \times 10^{-3}$	$5.73 \times 10^{-3}$
6.8	$8.3 \times 10^{-6}$	$-0.46 \times 10^{-3}$	$3.31 \times 10^{-3}$

<sup>a</sup> Definitions are as in table 1.

Table 3

Energy of excited-state hydrogen atom with perfectly imaging wall <sup>a,b</sup>

$L$ <sup>c</sup>	$-E(2p,  m  = 1)$ <sup>d</sup>	$-E(2s)$ <sup>e</sup>	$-E(2p, m = 0)$ <sup>f</sup>
1.05	0.266	0.2716	0.2548
1.5	0.1980	0.2100	0.1926
2	0.1626	0.1785	0.1527
2.5	0.1468	0.1620	0.1288
3	0.1403	0.1523	0.1144
3.5	0.1376	0.1459	0.1046
4	0.1363	0.1415	0.1015
4.5	0.1355	0.1383	0.1060
5	0.1348	0.1358	0.1130
5.5	0.1340	0.1340	0.1195
6	0.1332	0.1326	0.1246
6.5	0.1323	0.1317	0.1279
7	0.1315	0.1318	0.1292
8	0.1300	0.1331	0.1285
9	0.1288	0.1330	0.1276
10.5	0.1274	0.1314	0.1267
12	0.1266	0.1295	0.1262

<sup>a</sup> States formed from the  $n = 2$  state of the isolated atom; the interaction energy is  $\Phi = E + 0.125$ .<sup>b</sup> Entries in atomic units.<sup>c</sup> Perpendicular distance of proton to the wall.<sup>d</sup> Energy for a 2-fold degenerate state, see section 6.2.<sup>e</sup> Energy for a state which evolves from the 2s state of the isolated atom, see sections 4.1 and 6.2.<sup>f</sup> Energy for a state which evolves from the 2p,  $m = 0$  state of the isolated atom, see sections 4.1 and 6.2.

### 6.3. Results of the calculations

#### 6.3.1. Ground state

The results for  $\Phi$ ,  $\mu$ , and  $Q$  for the ground state of the model defined in eqs. (2.8) to (2.12) are presented in table 1.

A clearly developed local minimum in  $\Phi$  is formed at  $L$  of approximately  $3.44 a_0$ , of depth  $4.28 \times 10^{-3}$  au, as shown in fig. 3.

The ground-state electron density is shown as contour plots in fig. 4 for three values of  $L$ . The values of  $L$  were chosen to be near the minimum in  $\Phi$  ( $L = 3.4$ ), in

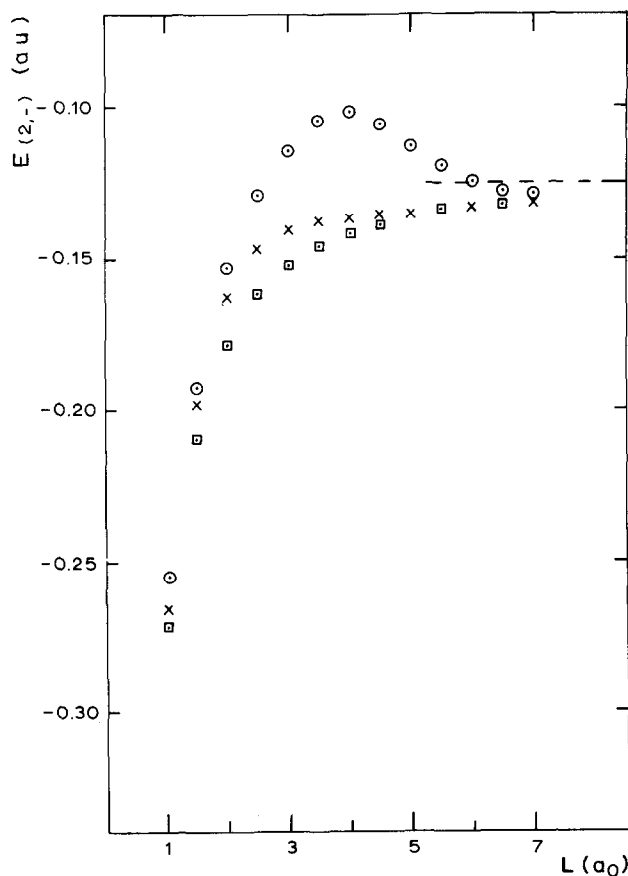


Fig. 5. Energies of the first 4 excited states, as a function of proton distance  $L$  from the wall. The energies were obtained from variational calculations described in section 6.2. The labelling of the states is discussed in section 4.1. The state  $2p, |m| = 1$  is 2-fold degenerate. Notice the absence of a potential barrier in all these states for  $L$  less than 2. Points are labelled by: x for  $2p, |m| = 1$ ; o for  $2p, m = 0$ ; □ for  $2s$ .

the region of strong repulsion between the atom and the surface ( $L = 1.6$ ) and in the region where the Van der Waals attraction to the surface becomes the dominant contribution to  $\Phi$  ( $L = 4.8$ ).

For use in the discussion and interpretation of these results, we performed the variational calculation also for the case of a hydrogen atom in the presence of an impenetrable wall; this differs from the above model by the omission of the image potential  $V_i$  from eq. (2.11). The results for the nonimaging wall model are presented in table 2. These data are discussed in sections 7 and 9, where the index "W" is used to identify them.

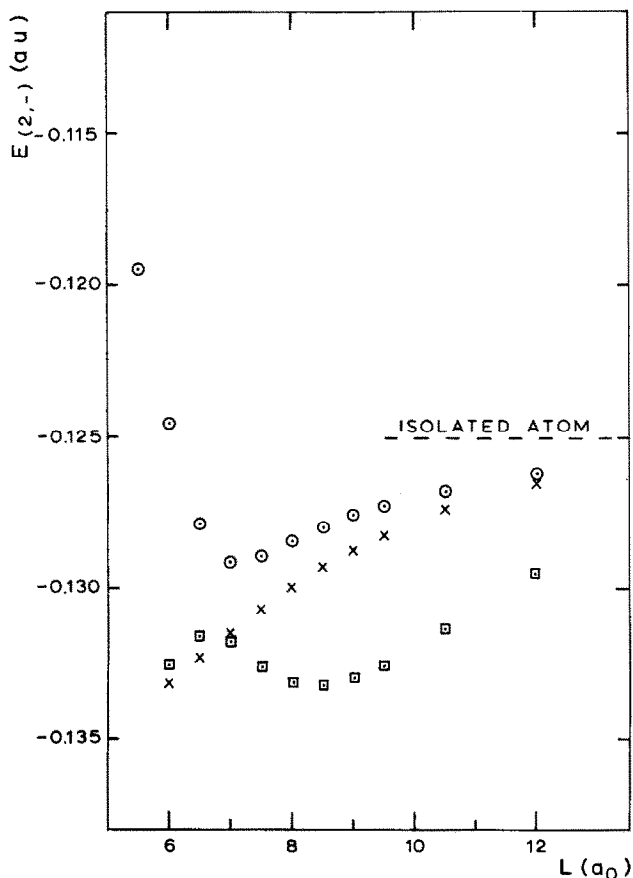


Fig. 6. Energies of the first 4 excited states, as a function of proton distance  $L$  from the wall. The identifications are as in fig. 5; the large- $L$  region is shown on an expanded scale here to display level crossings and the formation of local potential minima.

### 6.3.2. Excited states

The results for the energies of the  $n = 2$  states are shown in figs. 5 and 6 and are listed in table 3.

Of the three energy functions shown in fig. 6, there is no local minimum in  $\Phi$  for the  $2p, m = \pm 1$  states; there is a clearly developed local minimum for the  $2p, m = 0$  state and a rather poorly developed local minimum in the  $2s$  state. The form of the energy function for the  $2p, m = 0$  state is similar to the form of  $\Phi$  for the ground state of the system.

These results are discussed in sections 7.2.4 and 9.3.

## 7. The transition to the dispersion-force limit

As discussed in section 3, simplifying features appear in the model at small and at large separations.

### 7.1. Small separations-ground-state energy

At very small separations, the dominant term in the interaction energy is the proton-image proton energy. The variational calculation of section 5 was performed to extend this picture to somewhat larger separations. From table 1 and fig. 2 we see that the results for the ground-state  $\Phi$  obtained with the trial function of eq. (6.1) supersede the variational results of section 5 at values of  $L$  near 1: both are upper bounds and the second calculation yields a lower barrier in  $\Phi$ . The lower bound construction of section 3.2 shows that there is a region of positive  $\Phi$ ; the use of yet more complex variational trial functions cannot cause the barrier to disappear from the calculated  $\Phi$ .

We believe that our calculations with eq. (6.1) give a reliable account of the barrier, so that the exact results for the model are close to these values: the barrier is approximately 0.1 au high and has an effective width of approximately  $2 a_0$ . The tunneling probability for a proton through the barrier is so small that henceforth we ignore the small- $L$  region as being a nonphysical artifact of the model which is well-separated from the local minimum in the holding potential.

### 7.2. Dispersion forces

The minimum in the ground-state interaction energy near  $3.4 a_0$  arises from a balancing of the contributions of an effective repulsion, eq. (2.12), and of the dispersion forces. The dispersion energy here arises from the correlated charge fluctuations of the adatom and their images. At large separations it can be evaluated with perturbation theory.

For our model the perturbation results are stated in section 4. For more realistic models there is a similar reduction in the complexity of the calculations by evaluat-



ing the dispersion terms using perturbation theory methods. We use the data of tables 1 and 2 to analyse the transition to the range of separations where the leading perturbation theory results are accurate representations of the contents of the model. The transition is traced in the interaction energy and in the dipole moment. A related question is on the approximate additivity of the dispersion energy calculated by perturbation theory and the overlap-repulsion energy [7,10, 34]; it is discussed again in section 9.4 in conjunction with the results of table 5.

### 7.2.1. The ground-state interaction energy

At large separations the combination  $-L^3\Phi$  should decrease monotonically with

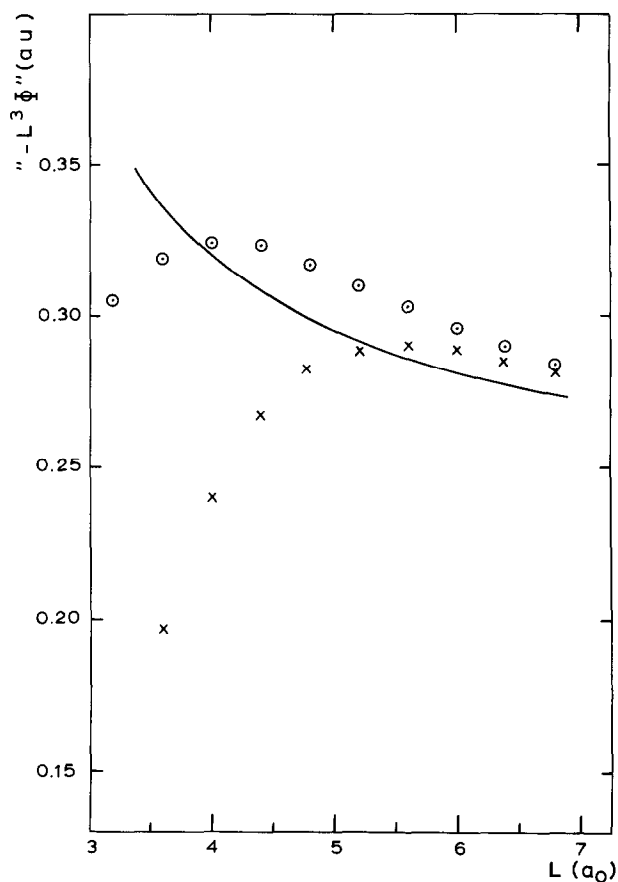


Fig. 7. Comparison of the ground-state interaction energy with the perturbation theory prediction. The solid curve is the combination  $-L^3\Phi^{(1)}$ , from eq. (4.8). The points  $\times$  denote  $-L^3\Phi$  formed from the data of table 1. The points  $\circ$  denote  $-L^3(\Phi - \Phi_W)$  formed from the data of tables 1 and 2. For discussion see section 7.2.1 of the text.

increasing  $L$ , according to the perturbation theory formula eq. (4.8). We show tests of this behaviour and a comparison with eq. (4.8) in fig. 7. In addition to the points which are formed from the data of table 1 there are points formed with a construction which tests the approximate additivity of the overlap and dispersion energies. These points are the combination  $-L^3(\Phi - \Phi_W)$ , in which the positive interaction energy of the nonimaging wall model (table 2) is subtracted from  $\Phi$ . If the processes were additive this would isolate the dispersion energy. Without the subtraction of  $\Phi_W$ , the transition to a region of monotone decrease occurs only for  $L$  larger than 5.5. With the subtraction the transition occurs near  $L = 4.5$ , which is markedly closer to the position of the potential minimum,  $L \approx 3.4$ .

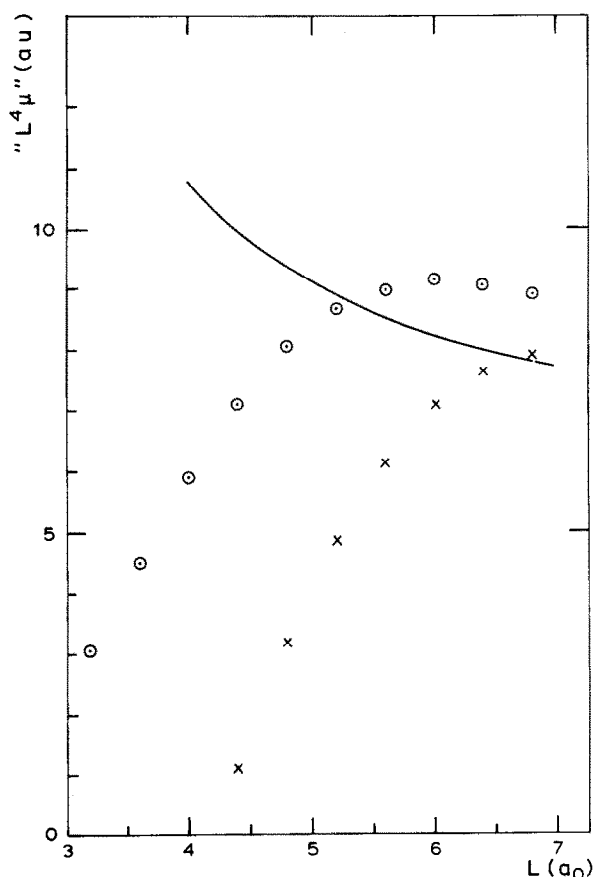


Fig. 8. Comparison of ground-state dipole moment with the perturbation theory prediction. The solid curve is the combination  $L^4\mu^{(1)}$ , from eq. (4.18). The points  $\times$  denote  $L^4\mu$  formed from the data of table 1. The points  $\circ$  denote  $L^4(\mu - \mu_W)$  formed from the data of tables 1 and 2. For discussion see section 7.2.2 of the text.

### 7.2.2. The dipole moment of the ground state

Antoniewicz noted [2] that in the leading order of perturbation theory the dispersion dipole moment is positive or directed outward. The positive sign is achieved in our model for  $L$  larger than 4.2.

According to eq. (4.18), the combination  $L^4\mu$  should decrease monotonically with increasing  $L$  at large  $L$ . Tests of this behaviour and a comparison with eq. (4.18) are shown in fig. 8. As in fig. 7, we attempt to isolate the dispersion contribution in the dipole moment by subtracting the nonimaging wall result (table 2) to form  $L^4(\mu - \mu^w)$ . Even with the subtraction the approach to the large  $L$ , leading perturbation theory result is slow; the region of monotone decrease sets in at values of  $L$  greater than 6.

The perturbation theory remains accurate for smaller  $L$  in the energy  $\Phi$  than in the dipole moment  $\mu$ .

### 7.2.3. The quadrupole moment of the ground state

The dispersion quadrupole moment is negative at large  $L$ , according to eq. (4.22). However, the perturbation series for  $Q$  is not dominated by its first terms even for  $L$  near 7. Further, an extension of the results in tables 1 and 2 shows  $Q_w$  for the nonimaging wall problem to be approximately 25% of the total  $Q$  at  $L = 7$ . Thus, simple trends in  $Q$  are not yet apparent at  $L = 7$ , apart from the sign being that predicted from perturbation theory.

### 7.2.4. The excited-state interaction energies

Perturbation-theory results for the interaction energies in states formed from the  $n = 2$  atomic states are given in eqs. (4.9) and (4.10). These only begin to approximate the results of the variational calculations, table 3, for values of  $L$  larger than 9. The ordering of the excited state energies is then the same as given by the perturbation results.

The crossing of energy levels shown in fig. 6 is not exceptional because the associated wave functions have different azimuthal symmetries.

## 8. Polarizability of the ground state

The polarizability of the adatom-substrate complex is characterized by a tensor with the two independent components defined in eq. (2.16): the response of the system in an electric field perpendicular to the surface,  $\alpha_{zz}$ , and the response for an electric field parallel to the surface,  $\alpha_{xx}$ . In calculating the depolarizing field in a simple two-dimensional lattice of adsorbed atoms (see section 9.2),  $\alpha_{zz}$  is the parameter needed.

For the perfect conductor model of the substrate used here, the perpendicular polarizability is a quantity observable in principle by application of a uniform field

perpendicular to the surface and measurement of the variation of the dipole moment with field strength. We mimic this with a calculation of  $\alpha_{zz}$  by the finite-field [16,17] method in which the variational calculation of section 6.1 is repeated with a Stark term added to the Hamiltonian eq. (2.9).

For the perfect conductor model, the definition of the parallel polarizability as the response for a uniform electric field parallel to the surface is not practical. Further, field ionization of the atom would occur in this geometry. Therefore, we work with the perturbation theory definition [16,17] of  $\alpha_{xx}$  for a localized charge distribution, eq. (2.16), and evaluate it by use of the Hylleraas variational principle [16,17,26]. The polarizability component  $\alpha_{xx}$  is thus determined by a perturbation procedure.

### 8.1. Perpendicular polarizability

In the finite-field method, we calculate the polarizability by taking the Hamiltonian to be

$$H(F) = H + F(z - L), \quad (8.1)$$

and repeating the multiparameter variational calculation to obtain the part of the dipole moment which is linear in the field  $F$ . For positive  $F$ , the Stark operator  $F(z - L)$  is bounded from below. If the field direction is reversed, we find that upon reoptimizing  $\alpha$  and  $\beta$  the trial energy can be driven arbitrarily negative, as discussed by Killingbeck [17].

We adjusted the linear and nonlinear parameters to minimize the trial energy for the  $N = 6$  (or  $N = 5$ , to similar accuracy) trial function of section 6.1 at three values of  $F$ , 0.001, 0.0025, and 0.005 au. The dipole moment for these fields is nearly linear in  $F$ , with zero field intercept equal to the values shown in table 1. Reoptimization of the parameters  $\alpha$  and  $\beta$  from their zero field values has negligible effect on the results when positive values of  $F$  are used.

Calculating the polarizability from the initial slope of  $\mu$  with  $F$  is equivalent to working with the second derivative of the trial energy with respect to  $F$  at zero field, because the Hellman–Feynman theorem remains valid [26] in a variational calculation such as ours.

The polarizability  $\alpha_{zz}$  for the model of eqs. (2.8) to (2.12) and  $\alpha_{zz}^w$  for the nonimaging wall model (omitting  $V_i$  from eq. (2.11)) are listed in table 4 and are shown in fig. 9.

### 8.2. Parallel polarizability

The parallel polarizability  $\alpha_{xx}$  defined in eq. (2.16) can be viewed as a second-order perturbation theory expression based on the exact spectrum (including the continuum) of the zero-field Hamiltonian. As such, the Hylleraas variational principle [16,17,26] facilitates its evaluation if the exact ground-state wave func-

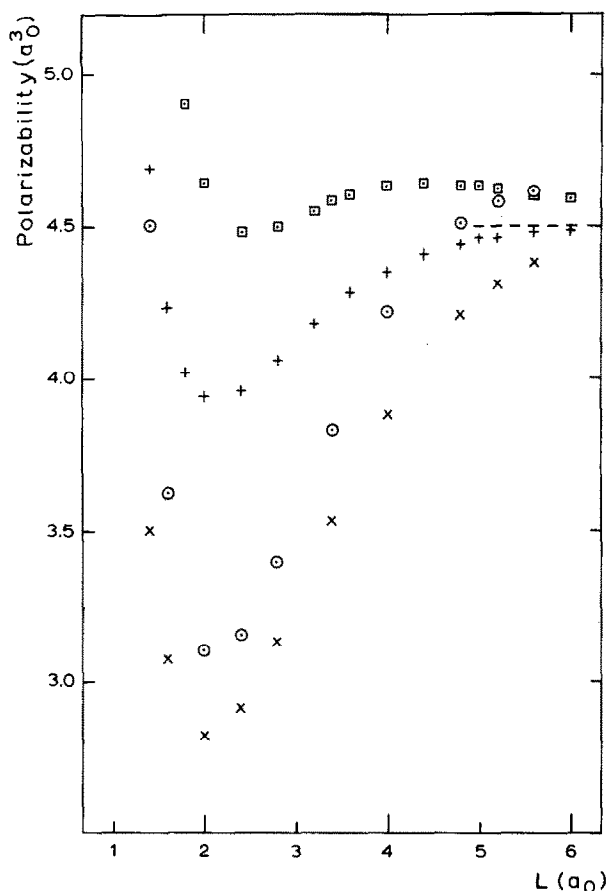


Fig. 9. Ground-state polarizability tensor components. The perpendicular ( $\alpha_{zz}$ ) and parallel ( $\alpha_{xx}$ ) polarizabilities are shown for the perfectly imaging wall ( $\circ$  and  $\square$ , respectively) and for the nonimaging wall ( $\times$  and  $+$ , respectively). The data are also listed in table 4. The polarizability of an isolated hydrogen atom is  $4.5 a_0^3$ . (For discussion, see section 8 of the text.)

tion is known. The polarizability  $\alpha_{xx}$  is to be obtained as the maximum of the functional

$$\alpha_{xx}^{(t)} = \{2(\psi, (E_0 - H) \psi) - 4(\psi_0, x\psi)\} / (\psi_0, \psi_0), \quad (8.2)$$

under variations of  $\psi$ , at fixed  $L$ .

For an approximate evaluation of  $\alpha_{xx}$ , which loses the rigorous bounding character of the calculation, we replace  $\psi_0$  in eq. (8.2) by the optimized trial function for the ground state obtained from eq. (6.1) with  $N=6$ . Then we use a trial function of the form of eq. (6.4) and its complex conjugate for the function  $\psi$ .

Table 4  
Polarizability of the hydrogen atom-substrate system <sup>a</sup>

<i>L</i>	$\alpha_{zz}$ <sup>b</sup>		$\alpha_{xx}$ <sup>c</sup>	
	$\alpha_{zz}$ <sup>d</sup>	$\alpha_{zz}^W$ <sup>e</sup>	$\alpha_{xx}$ <sup>d</sup>	$\alpha_{xx}^W$ <sup>e</sup>
1.2	6.64	4.40	— <sup>f</sup>	— <sup>f</sup>
1.4	4.50	3.50	6.62	4.69
1.6	3.62	3.07	5.44	4.23
1.8	— <sup>f</sup>	— <sup>f</sup>	4.90	4.02
2.0	3.10	2.82	4.64	3.94
2.4	3.15	2.91	4.48	3.96
2.8	3.39	3.13	4.50	4.06
3.2	— <sup>f</sup>	— <sup>f</sup>	4.55	4.18
3.4	3.83	3.53	4.58	— <sup>f</sup>
3.6	— <sup>f</sup>	— <sup>f</sup>	4.60	4.28
4.0	4.22	3.88	4.63	4.35
4.4	— <sup>f</sup>	— <sup>f</sup>	4.64	4.41
4.8	4.51	4.21	4.63	4.44
5	— <sup>f</sup>	— <sup>f</sup>	4.63	4.46
5.2	4.58	4.31	4.62	4.46
5.6	4.61	4.38	4.60	4.48
6.0	— <sup>f</sup>	— <sup>f</sup>	4.59	4.49

<sup>a</sup> All entries are in atomic units: the distance unit is  $1 a_0 \approx 0.529 \text{ \AA}$ , the polarizability unit is  $1 a_0^3 \approx 0.1482 \text{ \AA}^3$ .

<sup>b</sup> Perpendicular polarizability calculated by the finite field method.

<sup>c</sup> Parallel polarizability calculated by the perturbation-variation method.

<sup>d</sup> Hydrogen atom with perfect imaging metal and impenetrable wall at distance  $L$  from the proton.

<sup>e</sup> Hydrogen atom with impenetrable wall at distance  $L$  from proton.

<sup>f</sup> No calculation performed in this case.

This leads to a series of approximate values of  $\alpha_{xx}$  which appears to converge rapidly to a limit (to within  $\frac{1}{2}\%$ ) as  $N$  is increased to 6. The value of  $\alpha_{xx}^{(t)}$  at  $N = 6$  is insensitive to changes of  $\alpha'$  and  $\beta'$  from the values of  $\alpha$  and  $\beta$  in the ground-state trial function.

The values obtained in this way for models with and without images,  $\alpha_{xx}$  and  $\alpha_{xx}^W$ , are shown in fig. 9 and listed in table 4.

### 8.3. Discussion

The polarizability of an isolated hydrogen atom is  $4.5 a_0^3$ ; the results for the polarizability components in table 4 are of this order of magnitude. The polarizability components  $\alpha_{xx}$  and  $\alpha_{zz}$  show an appreciable anisotropy in the region of the local minimum in  $\Phi$ ,  $L$  near 3.4. The component  $\alpha_{zz}$  which enters in treatments of

depolarizing fields (see section 9.2) is decreased by 15% from the isolated atom value.

We now discuss the departures of  $\alpha_{xx}$  and  $\alpha_{zz}$  from the isolated atom value in terms of the mechanisms discussed for the ground-state properties in section 7.

Consider the effective polarizability [35] of a point "atom" of isolated polarizability  $\alpha_0$  at a distance  $L$  from a planar perfectly imaging substrate. Then the components  $\alpha_{zz}^{(i)}$  and  $\alpha_{xx}^{(i)}$  are expected to be unequal and to be both greater than  $\alpha_0$ . When the classical response is calculated, including the reinforcing fields of the induced image dipoles, the components are

$$\begin{aligned}\alpha_{zz}^{(i)} &= \alpha_0 / [1 - (\alpha_0/4L^3)] , \\ \alpha_{xx}^{(i)} &= \alpha_0 / [1 - (\alpha_0/8L^3)] .\end{aligned}\tag{8.3}$$

The data in table 4 do show  $\alpha_{xx}$  and  $\alpha_{zz}$  to be larger than  $\alpha_0$  ( $=4.5$ ) at large  $L$ , where the image charge effects in the dispersion terms give the dominant distortions of the ground state from the isolated atom ground state, section 7.2. However, the magnitude of the increase of the polarizability is less than would be calculated from eq. (8.3). There is only an indication in table 4 of a region of  $L$  greater than 5.6 where  $\alpha_{zz}$  would be significantly larger than  $\alpha_{xx}$ .

As the values of  $\alpha_{xx}$  and  $\alpha_{zz}$  are traced below  $L = 5$  in table 4, both decrease, and then increase again for small  $L$  values. We attribute the decrease to the increased rigidity of the charge distribution in the presence of the wall, and most of the increase we attribute to image effects becoming dominant again at small  $L$  values. This interpretation is supported by the trend of the nonimaging wall values,  $\alpha_{xx}^W$  and  $\alpha_{zz}^W$  in table 4. The rise in  $\alpha_{xx}^W$  and  $\alpha_{zz}^W$  at small  $L$  we attribute to another effect, visible in the ground-state electron distributions shown in fig. 4. At small  $L$  values (the effect is visible in fig. 4 at  $L = 1.6$ ), the electron density has a part which is significantly displaced from the proton and which therefore is able to respond much more freely than in the isolated atom. Thus, the effect of the wall over most of the range of  $L$  in table 4 and fig. 9 is to increase the rigidity of the atomic charge distribution. At small  $L$ , the ground-state density is modified enough by the presence of the wall to have a component which is quite polarizable.

While the existence of the competing processes which we have identified in the results could be recognized without detailed calculations, the quantitative treatment of the model shows that the balance between the processes alters in a marked way as the distance  $L$  varies.

## 9. Relation to the modelling of experiments

Because of the simplifications made in the construction of the basic model, eqs. (2.8) to (2.12), we do not attempt a quantitative comparison between the detailed results of sections 6 through 8 and experimental data on physisorbed atoms. How-

ever, the physical processes which we have attempted to incorporate in the model are believed to be the dominant processes in many physisorbed systems. In this section we review the results of sections 6 through 8, with an emphasis on the relation to models used in the interpretation of experimental data.

### 9.1. Holding potential of a physisorbed atom

Most discussions of the motion of physically adsorbed atom at a surface are based on the Born–Oppenheimer approximation [12], in which the nuclear motion occurs adiabatically on the ground-state electronic energy surface. This surface is the function  $E_0(L)$  in our model. There are crossings of the energy surfaces for excited electronic states of different azimuthal symmetries, as shown in the results in table 3. Such crossings may lead in some cases to significant corrections to the lowest-order adiabatic description of the motions of excited-state adatoms.

The local minimum in the holding potential  $\Phi$  of the ground-state atom, in table 1 and fig. 3, is slightly shallower than the strength of the Lennard-Jones polarization potential ( $1/L^3$ ) evaluated in the region of the minimum. This is in accord with our view of the minimum being formed by a balance between the polarization potential [18] and an overlap repulsion with the substrate electrons which is a sharply increasing function of decreasing distance  $L$ . It goes counter to an approximate calculation by van Himbergen and Silbey [9] for adsorbed inert gases which found a much stronger attractive potential than anticipated from an extrapolation of the polarization potential.

The holding potential  $\Phi(L)$  is obtained from our calculations as a numerical table. We found a good fit to the potential well with a Morse-hybrid potential:

$$V(L) = \begin{cases} \epsilon [\exp(2c[1 - L/L_0]) - 2 \exp(c[1 - L/L_0])] , & L < 5.32 , \\ -(0.25/L^3) - (1.125/L^5) , & L \geq 5.32 , \end{cases} \quad (9.1)$$

with  $\epsilon = 4.28 \times 10^{-3}$  au,  $L_0 = 3.445 a_0$ , and  $c = 2.488$ . The hybrid potential  $V(L)$  is continuous and has a continuous first derivative. Constructions we made using 3-parameter models [36] other than the Morse potential yielded less satisfactory fits to the numerical data.

Energy levels for perpendicular ( $z$  direction) motion of an adatom in the holding potential have been derived from selective adsorption molecular beam experiments [37–39]. We therefore determined the number and location of such levels for the model potential of eq. (9.1).  $V(L)$  is taken to be the potential for hydrogen atom motion at all separations  $L > 0$ , with an infinite barrier against atomic penetration into the substrate. Thus, the structure in  $\Phi$  found at  $L$  values less than  $1 a_0$  is omitted; we consider it be an unphysical aspect of the model which results from a too-literal application of image-charge fields at small charge–substrate separations.

There are 12 bound states for motions perpendicular to the surface. This number



was obtained by integrating the Schrödinger equation,

$$-(1/3672) \frac{d^2}{dL^2} \psi + V(L) \psi = E\psi, \quad (9.2)$$

at zero energy,  $E = 0$ , and counting the number of nodes [40] in  $\psi$ . The absolute values of the energies of the lowest 8 states are (all with an uncertainty of  $5 \times 10^{-6}$  au):  $3.525 \times 10^{-3}$ ,  $2.265 \times 10^{-3}$ ,  $1.2885 \times 10^{-3}$ ,  $6.55 \times 10^{-4}$ ,  $2.95 \times 10^{-4}$ ,  $1.15 \times 10^{-4}$ ,  $3.5 \times 10^{-5}$  and  $1.5 \times 10^{-5}$ . The total number of bound states found by counting the nodes agrees with an estimate obtained using the extrapolation procedure of LeRoy and Bernstein [41]. As in other examples [37–39] most of the bound states have such small energies that it is difficult to resolve them in selective adsorption experiments. This also makes it difficult to use [39,42] the experiments to determine the strength of the polarization potential.

### 9.2. Changes of work function with adsorbate coverage

The dipole moments of adatom–metal complexes have been derived from the change of the work function of the metal with adsorbate coverage. In one analysis of such data [43], the dipole moment per adatom was found to vary with surface coverage. Such a variation is expected to occur because the dipole moment of the adatom is reduced by the depolarizing fields of the other adatoms.

In the case of xenon adsorbed on palladium, Palmberg [43] estimated the polarizability of the adatom–metal complex to be twice the polarizability of an isolated xenon atom. As noted by Antoniewicz [12], a part of the effective polarizability can be attributed to the depolarizing fields of the induced image dipoles; we present a generalized form of the Antoniewicz argument [12] in Appendix A.

The polarizability component which enters in the calculation of depolarizing fields in a simple two-dimensional lattice [43] is  $\alpha_{zz}$ . In the region of the minimum of the holding potential, our model has values of  $\alpha_{zz}$  which are reduced from the isolated atom value by 15%. There is no evidence in our model for major increases in the polarizability at intermediate atom–surface separations.

The dipoles of heavy inert gases adsorbed on metals are found to be positive or directed outward. The dipole moment for our model is negative, or directed inward, in the region of the minimum of the holding potential although the dispersion theory contribution eq; (4.18) does become the dominant term at larger separations. Zaremba and Kohn have suggested [10] that the balance between the processes determining the orientation of the dipoles of physisorbed atoms is different for light and heavy atoms. The sign found in our model may yet be found to be the physical sign for few-electron atoms.

### 9.3. Excited-state interactions

Some discussions [44] of mechanisms for electron-impact desorption of atoms adsorbed on metals rely on qualitative features of the interaction energies of

electronically-excited adatoms with the metal. There is interest in whether the excited-state interaction curves at the separation of the minimum of the ground-state holding potential have repulsive branches.

In the states formed from the  $n = 2$  atomic states in our model, all the interactions at  $3.4 a_0$  are on strongly attractive branches. There are no repulsive branches at smaller  $L$ , a phenomenon we believe is similar to the small  $L$  behaviour of the ground state discussed in section 3.1. We do not know whether the behaviour of the excited states of the model at  $3$  to  $4 a_0$  is made nonphysical by the failure of image charge methods at small separations. However, according to the perturbation theory of section 4.1 the dispersion energy terms are much larger in these states than in the ground state.

We did not calculate the transition rate for radiative decay [45] from these excited states to the ground state.

#### 9.4. Interaction of atomic hydrogen with lithium fluoride

We have not identified a metal for which our model of hydrogen atom-metal interaction should be quantitatively accurate. However, the assumptions of a sharp substrate boundary and high characteristic substrate frequencies may be fulfilled for some alkali halides. Features of the holding potential for a hydrogen atom on lithium fluoride have been obtained [37] from the energy levels observed in selective adsorption. Here we present the results of a calculation for a modification of the model intended to resemble H/LiF.

The modification of the Hamiltonian to mimic a hydrogen atom interacting with a dielectric is to assign a factor  $(\epsilon - 1)/(\epsilon + 1)$  to the image term  $V_i$  in the electrostatic potential  $V$  of eq. (2.11).  $\epsilon$  is an effective dielectric constant, which is adjusted to be an average of the frequency-dependent function of the physical system. For an alkali halide, the actual dielectric constant has marked frequency dependence so that there is some arbitrariness in the choice of  $\epsilon$ .

We choose  $\epsilon$  by fitting the coefficient  $C_3$  of the Lifshitz polarization potential [18] evaluated [20] using optical data for H/LiF so that the leading perturbation theory term in  $\Phi$  is reproduced by the model:

$$C_3 = \frac{1}{4}(\epsilon - 1)/(\epsilon + 1). \quad (9.3)$$

The value of  $C_3$  obtained from experimental data for the optical constants of the atom and substrate is 0.048 au. We use

$$(\epsilon - 1)/(\epsilon + 1)|_{\text{H/LiF}} = 0.2. \quad (9.4)$$

The ground-state calculations for this dielectric model are made in the way described in section 6.1. The results for  $\Phi$  are shown in table 5. In the region of the potential minimum, values of  $L$  from 4.4 to  $7 a_0$ , these results are matched to within 10% by a simple estimate based on the numerical data of section 6. The estimate is formed by adding the nonimaging wall potential  $\Phi_W$  of table 2 to a dispersion-

Table 5  
Interaction of hydrogen atom with dielectric wall <sup>a,b</sup>

$L$	$\Phi_{\epsilon}^c$	$\Phi_{\text{est}}^d$	$\mu^e$
2.8	$7.828 \times 10^{-3}$		-0.112
3.2	$3.432 \times 10^{-3}$		$-6.85 \times 10^{-2}$
3.6	$1.314 \times 10^{-3}$		$-4.66 \times 10^{-2}$
4.0	$3.368 \times 10^{-4}$	$+3.1 \times 10^{-5}$	$-2.32 \times 10^{-2}$
4.4	$-8.30 \times 10^{-5}$	$-7.6 \times 10^{-5}$	$-1.27 \times 10^{-2}$
4.8	$-2.388 \times 10^{-4}$	$-2.22 \times 10^{-4}$	$-6.55 \times 10^{-3}$
5.0	$-2.665 \times 10^{-4}$		$-4.57 \times 10^{-3}$
5.2	$-2.756 \times 10^{-4}$	$-2.60 \times 10^{-4}$	$-3.10 \times 10^{-3}$
5.4	$-2.729 \times 10^{-4}$		$-2.02 \times 10^{-3}$
5.6	$-2.631 \times 10^{-4}$	$-2.50 \times 10^{-4}$	$-1.25 \times 10^{-3}$
6.0	$-2.336 \times 10^{-4}$	$-2.24 \times 10^{-4}$	$-3.1 \times 10^{-4}$
6.4	$-2.01 \times 10^{-4}$	$-1.94 \times 10^{-4}$	$+1.4 \times 10^{-4}$
6.8	$-1.71 \times 10^{-4}$	$-1.66 \times 10^{-4}$	$+3.1 \times 10^{-4}$

<sup>a</sup> Atomic units.

<sup>b</sup> Model with image charge strength 0.2, defined in section 9.4.

<sup>c</sup> Ground state interaction; as in table 1.

<sup>d</sup> Estimate of  $\Phi$  according to eq. (9.5).

<sup>e</sup> Dipole moment, as in table 1.

theory attraction obtained by multiplying the perturbation energy of eq. (4.8) by 0.2, which is the strength of the image charges:

$$\Phi_{\text{est}} = \Phi_W + 0.2 \Phi^{(1)}. \quad (9.5)$$

The success of this simple procedure is encouraging for the prospects of similar constructions which have been proposed [8,10] for physisorption holding potentials. Similar constructions have been used also for isolated pairs of inert gas atoms [34].

The depth of the holding potential quoted [37] for H/LiF is 18 meV ( $6.6 \times 10^{-4}$  au); our value calculated for the dielectric model is  $2.8 \times 10^{-4}$  au. The position of the potential minimum relative to the substrate boundary is not derived directly from the experimental data, but a model fitting some aspects of the data put [37] the location at 2.7 Å ( $5.1 a_0$ ) above the centers of the topmost layer of atoms. Our value of 5.2  $a_0$  from the wall translates to a much larger value than this, even allowing for some uncertainty in specifying the location of the imaging surface relative to the atomic positions in an insulator [19].

Even with the specification of the parameter  $\epsilon$  by eq. (9.4), we only achieve a qualitative agreement with the experimental data. Perhaps the discrete ionic character of the substrate is important in determining the depth of the holding potential minimum.

## 10. Conclusions

We have shown that a local minimum in the holding potential, of the order-of-magnitude of energies encountered in physical adsorption, is formed for our model of atomic hydrogen adsorption. The minimum is formed by a balance between the attractive polarization potential, studied by Lennard-Jones, and the overlap repulsion with the substrate, modelled here by a condition that the atomic electron is excluded from the substrate.

We have emphasized two areas in which increased information could lead to improvements upon the model: (1) For small charge—surface separations the potential energy for physical systems deviates from the value calculated with image charge fields. (2) The overlap repulsion between the atomic electron and the substrate electrons arises in a region where the probability densities of both species are nonzero; for this one must consider a diffuse boundary for the substrate rather than the mathematical plane used here.

We have given a brief comparison of our results with experimental data; increased experimental data could help to identify the points where effort at an improved model should be focussed. The poor quantitative agreement of the calculation to model hydrogen on lithium fluoride may reflect, in part, the ionic character of the substrate. Perhaps determining the holding potential for physical adsorption on a nonionic insulator would be a simpler test of the model. The balance of processes in the dipole moment and polarizability of the hydrogen atom has been traced: work function data for physisorbed few-electron atoms would give useful information for guiding extensions of this work.

We have discussed the relation of our results to the methodology of intermolecular force theory. Perturbation theory for the ground-state energy and the dipole moment was found to be fairly accurate for proton-surface distances down to  $1.5 L_0$ ,  $L_0$  being the distance of the holding potential minimum. An approximate additivity was found for the competing processes in the holding potential; it was illustrated with the hydrogen—lithium fluoride model.

We have presented a one-electron model for physical adsorption. It is a simplification of the complex many-electron problem of adsorption. It provides an instance where processes discussed in qualitative terms for complex systems can be followed quantitatively as parameters of the model are varied. It may serve to sharpen the understanding of these processes.

## Appendix A: Image charge contributions to depolarizing fields

If image charge terms are included in the Hamiltonian of charged particles in the presence of a dielectric, it is plausible that image charge fields will contribute to the expectation values of dipoles induced in the charge distributions. Antoniewicz [12] confirmed this assertion in a Drude model calculation. Here we show how the

assertion is proved with a perturbation theory for two well-separated charge distributions.

We calculate the depolarizing fields for two hydrogen atoms, labelled *a* and *b*, in the presence of a perfectly-imaging metal substrate. The argument is easily generalized to many-electron atoms. Assume the solutions for the ground-state energy and wave function of the single atom—substrate problems are known:

$$H_a \psi_a = E_0(a) \psi_a, \quad H_b \psi_b = E_0(b) \psi_b. \quad (\text{A.1})$$

The wave functions  $\psi_a$  and  $\psi_b$  in general describe charge distributions with net electric dipole moments.

When the two atoms are well-separated, the electrostatic interaction between the charge distributions, including image terms, can be expanded with a multipole series. The leading term is the dipole—dipole interaction:

$$V_{dd} = -\boldsymbol{\mu}_a \cdot \boldsymbol{T}_{ab} \cdot \boldsymbol{\mu}_b - \boldsymbol{\mu}_a \cdot \boldsymbol{T}_{ab'} \cdot \boldsymbol{\mu}_{b'}. \quad (\text{A.2})$$

$\boldsymbol{\mu}_a$  and  $\boldsymbol{\mu}_b$  are dipole moment operators for the charge distributions of atoms *a* and *b*;  $\boldsymbol{\mu}_{a'}$  and  $\boldsymbol{\mu}_{b'}$  are dipole moment operators for the image charge distributions, given in terms of  $\boldsymbol{\mu}_a$  and  $\boldsymbol{\mu}_b$  by the rules for the construction of images. The tensor  $T_{ij}$  is the dipole tensor linking distributions separated by a vector distance  $R_{ij}$ :

$$T_{ij} = (1/R_{ij}^3) \{ 3(R_{ij} R_{ij} / R_{ij}^2) - 1 \}. \quad (\text{A.3})$$

We emphasize that although a multipole series is used in forming  $V_{dd}$ , no such expansion is implicit in eqs. (A.1). The perturbation theory we use is based on the two atoms being well-separated; they both may be strongly perturbed by the substrate.

For large separations of the two atoms, the Schrödinger equation for the two-atom problem is approximately

$$(H_a + H_b + V_{dd}) \Psi = E \Psi. \quad (\text{A.4})$$

If  $V_{dd}$  is treated as a perturbation, there is a series for the ground-state wave function

$$\Psi_0 \simeq \psi_0 + \psi_1 + \dots, \quad (\text{A.5})$$

with  $\psi_0 = \psi_a \psi_b$ , and

$$\psi_1 = [(1 - P_0)/(E_0(a) + E_0(b) - H_a - H_b)] V_{dd} \psi_0. \quad (\text{A.6})$$

The dipole moment on atom *a* is

$$\langle \boldsymbol{\mu}_a \rangle = (\Psi_0, \boldsymbol{\mu}_a \Psi_0) / (\Psi_0, \Psi_0) = (\boldsymbol{\mu}_a)_0 + (\boldsymbol{\mu}_a)_1 + \dots, \quad (\text{A.7})$$

where

$$(\boldsymbol{\mu}_a)_0 = (\psi_a, \boldsymbol{\mu}_a \psi_a) / (\psi_a, \psi_a) \quad (\text{A.8})$$

is the dipole moment of the single atom–substrate complex and

$$(\mu_a)_1 = 2(\psi_0, \mu_a \psi_1) / (\psi_0, \psi_0) \quad (\text{A.9})$$

is the leading change in the dipole moment caused by the presence of the second complex.

The first-order perturbation term in eq. (A.9) factors because no excited states of the b-system occur in the intermediate sum over states when it is written as a matrix product. Hence, the first order term is written

$$\begin{aligned} (\mu_a)_1 &= -2(\psi_a, \mu_a [(1 - P_0)/(E_0(a) - H_a)] \mu_a \psi_a) \cdot [T_{ab'}(\mu_b)_0 + T_{ab'} \cdot (\mu_{b'})_0] \\ &= \alpha_a \cdot [T_{ab} \cdot (\mu_b)_0 + T_{ab'} \cdot (\mu_{b'})_0] . \end{aligned} \quad (\text{A.10})$$

The tensor  $\alpha_a$  of eq. (A.10) is the (generally anisotropic) polarizability tensor of system a; for the hydrogen atom the definition implicit in eq. (A.10) is the same definition used in eqs. (2.16).

The terms on the right-hand-side of eq. (A.10) have a direct interpretation as the classical fields of the dipole and image dipole of atom b.

There are quantum corrections to this classical result for calculating the depolarizing field. They occur in higher orders of the perturbation theory and are higher order in the inverse atomic spacing.

## Acknowledgements

One of us (L.W.B.) thanks the members of the Instituut voor Theoretische Fysica for their support and their hospitality. We thank Drs. C. Stolk and M. Lemoine for assistance with the computer programming.

## References

- [1] J.E. Lennard-Jones, *Trans. Faraday Soc.* 28 (1932) 334.
- [2] P.R. Antoniewicz, *Phys. Rev. Letters* 32 (1974) 1424.
- [3] E.g., discussion of J.R. Schrieffer, in: *Proc. Inter. School of Physics Enrico Fermi, Course LVIII: Dynamic Aspects of Surface Physics* (Italian Physical Society, Bologna, 1974) p. 250 ff.
- [4] T.B. Grimley, in: *Progress in Surface and Membrane Science*, Vol. 9, Eds. D.A. Cadenhead, J.F. Danielli and M.D. Rosenberg (Academic Press, New York, 1975).
- [5] S.C. Ying, J.R. Smith and W. Kohn, *Phys. Rev. B* 11 (1975) 1483.
- [6] N.D. Lang and A.R. Williams, *Phys. Rev. Letters* 34 (1975) 531.
- [7] G.G. Kleiman and U. Landman, *Solid State Commun.* 18 (1976) 819.
- [8] A.C. Hewson and D.M. Newns, *Japan. J. Appl. Phys. Suppl.* 2, Pt. 2 (1974) pp. 121–130; J.P. Muscat and D.M. Newns, *Phys. Letters* 61A (1977) 481.
- [9] J.E. van Himbergen and R. Silbey, *Solid State Commun.* 23 (1977) 623.
- [10] E. Zaremba and W. Kohn, *Phys. Rev. B* 15 (1977) 1769.

- [11] Compare ref. [2] with the increased complexity of:  
E. Zaremba, Phys. Letters 57A (1976) 156;  
B. Linder and R.A. Kromhout, Phys. Rev. B13 (1976) 1532.
- [12] P.R. Antoniewicz, Phys. Status Solidi (b) 86 (1978) 645; we do not find the anomalous depolarizing field for anisotropic molecules discussed by Antoniewicz.
- [13] E. Teller and H.L. Sahling, in: Physical Chemistry; An Advanced Treatise, Vol. 5, Ed. H. Eyring (Academic Press, New York, 1970).
- [14] This follows the conventions of J.D. Jackson, Classical Electrodynamics (Wiley, New York, 1975).
- [15] There is a factor  $1/2$  different in the definition used by A.D. Buckingham, in: Advances in Chemical Physics, Vol. 12 (Wiley, New York, 1967).
- [16] A. Dalgarno, Advan. in Phys. 11 (1961) 281.
- [17] J.P. Killingbeck, Phys. Letters 65A (1978) 180;  
J.P. Killingbeck, Rept. Progr. Phys. 40 (1977) 963.
- [18] E.M. Lifshitz, Zh. Eksperim. i Teor. Fiz. 29 (1954) 94; Soviet Phys.-JETP 2 (1956) 73.  
Yu.S. Barash and V.L. Ginzburg, Usp. Fiz. Nauk 116 (1975) 5; Soviet Phys.-Usp. 18 (1975) 305.
- [19] E. Zaremba and W. Kohn, Phys. Rev. B13 (1976) 2270.
- [20] L.W. Bruch and H. Watanabe, Surface Sci. 65 (1977) 619.
- [21] N.D. Lang and W. Kohn, Phys. Rev. B7 (1973) 3541.
- [22] M.W. Cole, Phys. Rev. B2 (1970) 4239.
- [23] L.K. Haines and D.H. Roberts, Am. J. Phys. 37 (1969) 1145.
- [24] R.F. Wallis, R. Herman and H.W. Milnes, J. Mol. Spectrosc. 4 (1960) 51.
- [25] Note that this value differs from the critical coupling constant for a finite-dipole potential in three dimensions, reviewed by J.E. Turner, Am. J. Phys. 45 (1977) 71, because of the half-space condition, eq. (3.6).
- [26] S.T. Epstein, The Variational Method in Quantum Chemistry (Academic Press, New York, 1974).
- [27] For an application of the image model to adsorbed molecular hydrogen see: F. Flores, N.H. March and I.D. Moore, Surface Sci. 69 (1977) 133.
- [28] We use a standard notation for the excited states; see, e.g., L. Pauling and E.B. Wilson, Introduction to Quantum Mechanics (McGraw-Hill, New York, 1935). This also reviews the calculations of the atomic polarizability.
- [29] A. Dalgarno and J.T. Lewis, Proc. Roy. Soc. (London) A233 (1955) 70.
- [30] Treated in various levels of sophistication by:  
C. Kocher, Am. J. Phys. 45 (1977) 71;  
L.D. Landau and E.M. Lifshitz, Quantum Mechanics (Pergamon, London, 1958) ch. VI;  
B. Simon, Ann. Phys. (NY) 97 (1976) 279.
- [31] M. Abramowitz and I.A. Stegun, Eds. Handbook of Mathematical Functions (Dover, New York, 1965).
- [32] J.H. Wilkinson, The Algebraic Eigenvalue Problem (Clarendon, Oxford, 1965).
- [33] S.H. Gould, Variational Methods for Eigenvalue Problems (Univ. of Toronto Press, Toronto Press, Toronto, 1957) section III.12.
- [34] E.g., J.N. Murrell and G. Shaw, J. Chem. Phys. 49 (1969) 4731.
- [35] W.C. Meixner and P.R. Antoniewicz, Phys. Rev. B13 (1976) 3276, and references contained therein.
- [36] D. Steele, E.R. Lippincott and J.T. Vanderslice, Rev. Mod. Phys. 34 (1962) 239.
- [37] H.U. Finzel, H. Frank, H. Hoinkes, M. Luschka, H. Nahr, H. Wilsch and U. Wonka, Surface Sci. 49 (1975) 577.
- [38] G. Boato, P. Cantini and R. Tatarek, Phys. Rev. Letters 40 (1978) 887.
- [39] G. Derry, D. Wesner, S.V. Krishnamurty and D.R. Frankl, Surface Sci. 74 (1978) 245.

- [40] Levinson's theorem, e.g. in K. Gottfried, *Quantum Mechanics*, Vol. I (Benjamin, New York, 1966) pp. 894–896.
- [41] R.J. LeRoy and R.B. Bernstein, *J. Chem. Phys.* 52 (1970) 3869.
- [42] R.J. LeRoy, *Surface Sci.* 59 (1976) 541.
- [43] P.W. Palmberg, *Surface Sci.* 25 (1971) 598.
- [44] H.H. Farrell, M. Strongin and J.M. Dickey, *Phys. Rev. B* 6 (1972) 4703;  
P.A. Redhead, *Can. J. Phys.* 42 (1964) 886;  
D. Menzel and R. Gomer, *J. Chem. Phys.* 41 (1964) 3311.
- [45] R.R. Chance, A.H. Miller, A. Prock and R. Silbey, *J. Chem. Phys.* 63 (1975) 1589, and references contained therein.